PROCEEDINGS A

royalsocietypublishing.org/journal/rspa

Research

Cite this article: Pednekar S, Krishnadas A, Cho B, Makris NC. 2023 Weber's Law of perception is a consequence of resolving the intensity of natural scintillating light and sound with the least possible error. *Proc. R. Soc. A* **479**: 20220626.
https://doi.org/10.1098/rspa.2022.0626

Received: 24 September 2022
Accepted: 3 March 2023

Subject Areas:
optics, acoustics

Keywords:
perception, Weber's Law, psychophysics, pattern recognition, just-noticeable-difference, Fechner

Author for correspondence:
Nicholas C. Makris
e-mail: makris@mit.edu

Electronic supplementary material is available online at https://doi.org/10.6084/m9.figshare.c.6472407.

THE ROYAL SOCIETY PUBLISHING

Weber's Law of perception is a consequence of resolving the intensity of natural scintillating light and sound with the least possible error

Shourav Pednekar, Arun Krishnadas, Byunggu Cho and Nicholas C. Makris

Department of Mechanical Engineering, Massachusetts Institute of Technology, Cambridge, MA 02139, USA

SP, 0000-0001-6412-887X; BC, 0000-0003-4926-2792; NCM, 0000-0003-4369-296X

Efficient resolution of natural light and sound intensity is essential for organisms, systems and machines that rely on visual and auditory sensory perception to survive or function effectively in their environment. This resolution obeys Weber's Law when the smallest resolvable change, a just-noticeable-difference, grows in direct proportion to the stimulus. Here, Weber's Law is found to be a consequence of attaining the theoretical minimum mean-square error possible, the Cramer–Rao lower bound, in resolving the intensity of naturally scintillating light and sound. The finding is based on statistics from thousands of measurements of naturally scintillating environmental light and sound signals. Remarkably, just-noticeable-differences in light and sound intensity measured over decades of psychophysical experiments with artificial sources are also found to approximately attain the respective Cramer–Rao lower bounds. Human intensity resolution is in this way optimally adapted to the natural scintillation of light and sound. Pattern recognition by simple matched-filter correlation between measured and hypothetical images cancels natural scintillation. For intensity perception obeying Weber's Law, this is found to be advantageous and statistically optimal because perceived scintillation is

independent of the underlying signal pattern. A small visual patch change or acoustic signature truncation is shown to be lost in natural signal-dependent fluctuations if perception with constant intensity resolution is attempted.

1. Introduction

Efficient resolution of naturally scintillating light and sound intensity is essential for organisms, systems and machines that rely on visual and auditory sensory perception to survive or function effectively in their environment. The reliable recognition of patterns imbedded in the scintillating intensities of natural light and sound is also indispensable for survival or proper function in many contexts. Optimizing the performance and efficiency of these crucial tasks in perception should provide advantages in a potentially competitive or hostile environment. Over many decades of psychophysical experiments, it has been shown that human resolution of artificially generated light and sound intensity approximately follows a relationship known as Weber's Law [1–12]. In Weber's Law, the smallest resolvable change in intensity, known as a just-noticeable-difference, is not constant but grows in direct proportion to the mean intensity stimulating a sensing system. In other words, intensity resolution seems to be intriguingly worse for larger intensities of light and sound and better for smaller ones. Various hypothetical internal mechanisms of a visual or auditory sensing system have been proposed to potentially account for the observation of Weber's Law or its empirical approximations in historic psychophysical measurements. These range from the neurological and physiological [13,14] to hypothetical internal system noise [15]. Recent reviews across diverse areas, however, note a lack of evidence for how Weber's Law may provide functional advantages in a variety of contexts [16,17].

Here, we explain how Weber's Law is extremely advantageous as an adaptation for sensing with naturally scintillating light and sound. We begin by determining the intensity scintillation [18] statistics of natural light and sound signals from thousands of environmental measurements. Over repeated samples of a natural scene measured with daylight or an acoustic signature generated with natural objects, intensity fluctuations are found at every pixel of the respective spatial image or temporal series. The fluctuations arise primarily from propagation and multiple scattering through and from the random atmosphere and terrestrial surfaces for images formed with daylight [18–21], and from randomness in the source mechanism for time series formed with sound [22]. This natural intensity scintillation is found to have a standard deviation, or resolution footprint, that grows in direct proportion to the mean, so following Weber's Law.

Interestingly, log-transformed intensity is found to have a standard deviation independent of mean intensity. Resolution is then constant in log-transformed intensity. By various approaches, log-transformation is found to be a variance-stabilizing transformation [23] given our scintillating light and sound data. That is, it transforms a random variable from having a variance that depends on the mean to one that has a variance independent of the mean [24]. This property helps log-transformed intensity converge from diverse physical mechanisms to a normal probability density via the central limit theorem [25]. Many of these mechanisms involve independent multiplicative factors arising from stochastic propagation, scattering or wave generation that become additive after log-transformation [18,20,26]. A normal probability density is advantageous because it only requires knowledge of the first two moments of the data, the mean and covariance which typically can be readily estimated, for a complete statistical description.

Fechner developed an approach for transforming physically measurable stimuli to a quantifiable variable that he argued is perceived by a human observer [1]. Fechner's transformation is based on his assumption that an external stimulus is perceived in a manner so that it has a constant resolution metric from the observer's perspective. The concept has intuitive appeal for those inclined to measure quantities with fixed rather than varying metrics, but may be counterintuitive if the metric arrived upon does not have simple physical units, such as intensity

which is power per unit area. Fechner's transformation employs a process known as Fechnerian-integration [1,6,27–29] of psychophysically measured just-noticeable-differences. The relevant just-noticeable-differences to this analysis were measured with artificial light and sound intensity stimuli [1–12]. From these, Fechner's transformation is remarkably found both theoretically and experimentally to be a variance-stabilizing transformation of the naturally scintillating light and sound intensity we measure. Fechner derived his transformation at an early date without use of statistical arguments, without connection to variance stabilization, and without consideration of the specific statistical fluctuations of the stimuli [1]. All of these, however, are necessary to explain how Weber's Law relates to optimal intensity resolution of natural scintillating light and sound and the benefits of this optimality.

Given the need for fundamental statistical resolution metrics, we turn to the Cramer–Rao lower bound [30]. The minimum mean-square error possible in the unbiased estimation of a parameter from random data cannot be smaller than this bound. The proof via Cauchy–Schwartz inequality was supplied by Rao [31] and Cramer [32] to support Fisher's earlier asymptotic analysis [33,34] that what is referred to as the Fisher information [30,34] is the inverse of this same bound. The bound is here used to assess the optimality of sensing the intensity of naturally scintillating light and sound with resolution obeying Weber's Law. We in fact find that sensing resolution should be constant in log, variance-stabilizing or Fechnerian transformed intensity, rather than in intensity itself to attain the Cramer–Rao lower bound in intensity estimation. Weber's Law is found to be a consequence of attaining this optimal intensity resolution given the natural scintillation of environmental light and sound we measure. Remarkably, just-noticeable-differences in intensity stimulus, from decades of psychophysical measurements with artificial sources [2–12], are also found to approximately attain the respective Cramer–Rao lower bounds. As change-detection thresholds rather than root-mean-square errors, the just-noticeable-differences are found to be in the optimal range of primarily rejecting natural fluctuations rather than true changes in mean intensity of environmental light and sound data. These findings show human intensity resolution to be approximately optimally adapted to the natural scintillation of light and sound.

Intensity perception obeying Weber's Law is found to have a number of other advantages given the natural fluctuations of environmental light and sound intensity. It enables information reception to be easily maximized and pattern recognition easily optimized according to criteria from information, estimation and detection theories [30,35–37]. For example, when intensity perception obeys Weber's Law, simple linear correlations between measured and hypothetical images, also known as matched filters [36], are found to be sufficient statistics [30,34,36] containing all necessary information in the data to determine which hypothetical pattern best matches the measured one. From a practical perspective, the correlation reinforces the mean signal perceived while cancelling perceived fluctuations. This is optimal when the perceived fluctuations do not contain signal information as is the case when intensity perception obeys Weber's Law. If intensity perception does not obey Weber's Law, but instead employs constant resolution for all intensities, cancelling fluctuations destroys signal information contained in the fluctuations and leads to suboptimal pattern recognition. This is demonstrated with a variety of examples using natural objects imaged in daylight and sounds made from natural sources where important environmental patterns are lost in natural scintillation when intensity perception does not follow Weber's Law.

Following general concepts from Darwinian evolution, a significant body of literature presents evidence or theories that biological sensory systems have been adapted to properties of signal information [38–45] encountered in the natural environment, including efficient coding of signal information [46–48]. That is done, however, without considering the natural intensity scintillation of the light and sound waves carrying the signal information. The analysis and conclusions presented here are distinct from that literature because we show the intensity scintillation of natural light and sound waves, irrespective of the signal information the waves carry, leads to correspondingly distinct adaptations for optimal sensing. Weber's Law, in this regard, is here found to be a consequence of sensing intensity with the smallest possible error where

the error is entirely due to the intensity scintillation of natural light and sound waves. Such scintillation, a form of signal-dependent noise, is pervasive in optical images of environmental scenes illuminated with natural daylight due to atmospheric fluctuations along the light's path of propagation and scattering. These fluctuations, for example, lead to the familiar twinkling starlight that motivates astronomers at great cost to place telescopes in orbit outside the earth's atmosphere to obtain scintillation-free signals. Such scintillation is also pervasive in natural sounds due to the stochastic source mechanisms by which they are generated.

Previous studies of intensity signals in noise in the context of biological sensing systems [15] have similarly not considered the natural intensity scintillation of the physical light and sound waves, but have suggested that hypothetical internal sensory system noise mechanisms of unknown origin may lead to Weber's Law. Our analysis and results show such internal system noise mechanisms are not necessary because Weber's Law can be entirely explained as a consequence of sensing the intensity of naturally scintillating sound and light waves with the minimum possible error.

2. Naturally scintillating sound intensity

To investigate the naturally occurring scintillation of environmental sounds, we conducted a series of experiments. Natural sounds important to survival for many animals that rely upon acoustic sensing for survival were measured. Sounds that would typically alert animals to nearby prey, potential predators or rivals, such as: disturbances to local plant cover; disturbances to water sources and animal vocalizations were selected to study scintillation statistics. For these respective categories, the sounds of: leaves rustling on brushing tree branches, a footstep on grass, a leafless branch rubbing against tree bark; a stick plunged into a stream and a mammalian vocalization were chosen for measurement and analysis since they generally occur in terrestrial ecosystems.

In these experiments, the acoustic event from a particular natural sound source with a characteristic signature is generated and recorded to form an intensity time series of the event. To unify the analysis of sound and light intensity data, consider the time series to essentially be a one-dimensional image with time samples referred to as pixels indexed in time. The event is repeatedly generated and recorded to obtain many independent samples of the entire event time series changed only by natural mechanisms in the event's random generation and reception. Statistical fluctuations of natural sound at each pixel in the intensity image are determined from these samples. The temporal, spatial and frequency samplings are selected to be consistent with those found for the human auditory system. The same process is used to characterize the signals and fluctuations of all sound sources considered.

The acoustic pressure time series of natural sounds in figure 1 was recorded with a NTI XL2 microphone at 48 kHz sampling rate with a flat frequency response in the audible range from 20 Hz to 20 kHz. The pressure time series of the acoustic event, namely leaves rustling by a short brushing of adjacent tree branches in a forest setting, is shown in figure 1*a*, with corresponding spectrogram in figure 1*b* and power spectral density in figure 1*c*. The rustling leaves event is generated and recorded repeatedly, $N = 154$ times. Each of the N pressure time series of the event is band pass filtered to the auditory system critical band of $1\,\text{kHz} \pm 64\,\text{Hz}$ [53]. From these, N intensity time series of different random samples of the rustling leaves event are formed by squaring pressure, dividing it by the acoustic impedance of air, and sequential averaging over time to 10 ms increments or pixel sizes. These independent intensity time series of the event $W_j(t)$ for time pixel t across random event sample $j = 1, 2, 3, \ldots, N$ then have temporal and spectral resolution similar to that of the human auditory system in the 1 kHz critical band [54].

Signal-dependent noise is seen when the time series of the sample mean intensity $\bar{W}(t)$ is plotted with the corresponding intensity standard deviation $\sigma_W(t)$ taken across the N independent random samples of the acoustic event (figure 1*d*). That is, the standard deviation is seen to grow in direct proportion to the mean, which is taken to bear the signal. The standard deviation is large when the mean is large, and commensurably smaller for smaller mean.

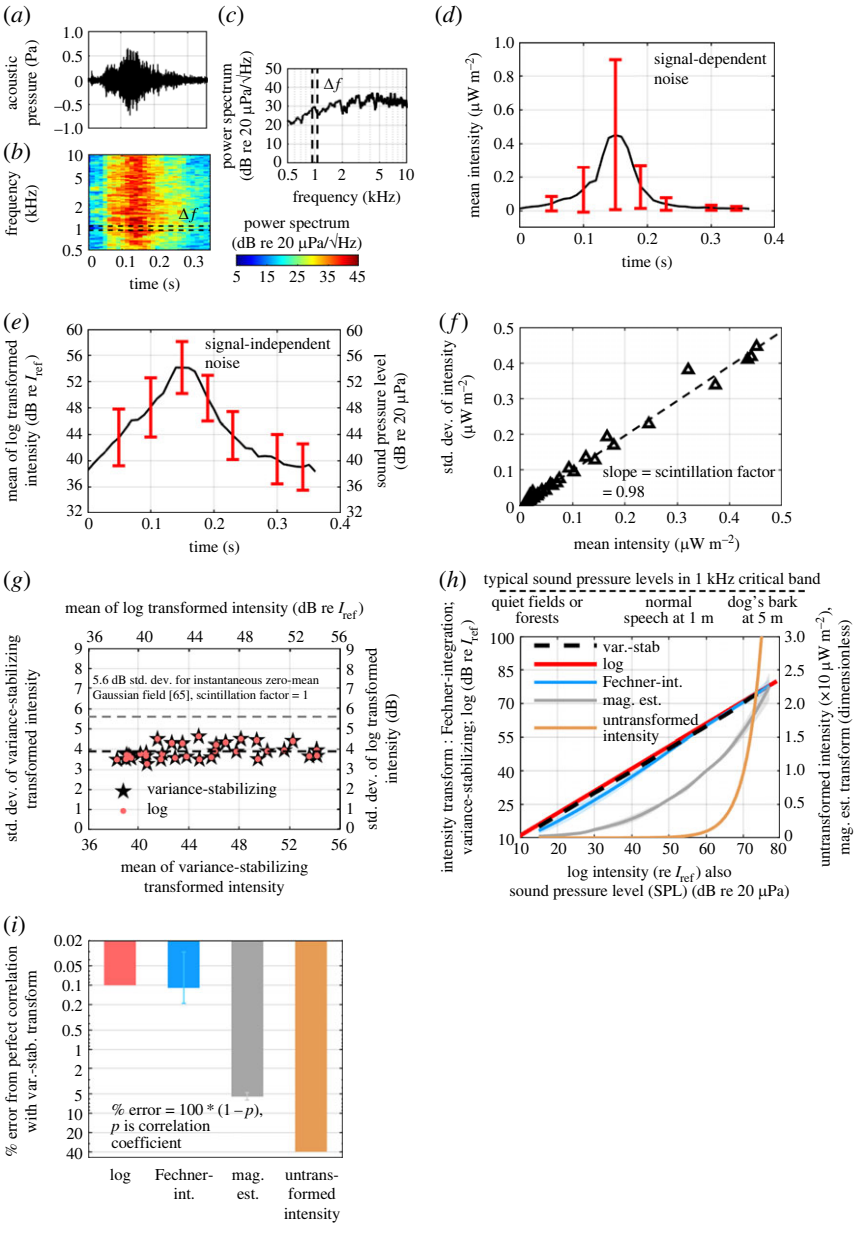

Figure 1. The sound of a rustling leaves event over time is measured repeatedly to determine the statistical properties of its intensity scintillation at every temporal pixel. (*a*) Raw acoustic pressure time series of a single measurement of the event with (*b*) corresponding spectrogram and (*c*) power spectral density. (*d–i*) Analysis over human auditory critical band of 128 Hz centred at 1000 Hz and pixel increment 10 ms: (*d*) mean acoustic intensity time series (black) over $N = 154$ event samples characterizes the event signal signature, with standard deviation (red) that varies in direct proportion to the local mean intensity. (*e*) Same as (*d*) but for log-transformed intensity which shows constant standard deviation (red) about mean (black), $I_{\mathrm{ref}} = P_{\mathrm{ref}}^2/\rho_a c_a$, $P_{\mathrm{ref}} = 20\ \mu\mathrm{Pa}$, $\rho_a = 1\ \mathrm{kg\ m^{-3}}$ and $c_a = 340\ \mathrm{m\ s^{-1}}$. (*f*) Intensity standard deviation as a function of mean intensity, as sorted across temporal pixels, shows direct proportionality. (*g*) Standard deviations of both log-transformed and variance-stabilizing transformed intensity are constant across their respective means. (*h*) Various intensity transformations as a function of log-transformed intensity. The variance-stabilizing transform is obtained from our measured acoustic data. Fechnerian transform and magnitude estimation transforms are derived from decades of independent psychophysical investigations filling the 128 Hz critical band centred at 1000 Hz with artificial sound sources [2–6,49–52]. (*i*) Deviation of various transformations from variance-stabilizing transformation dependence on mean intensity. Intensity transformation curves in (*h*) are used to calculate the cross-correlation coefficient [30] ρ, and the percentage error $100(1 - \rho)$. Similar results are found for other natural sounds (electronic supplementary material, figure S1).

Interestingly, the situation changes after log-transformation (figure 1*e*). The standard deviation is a constant function of the mean, so signal-dependent noise is not seen in the time series of the corresponding plot of the sample mean $\overline{\mathcal{T}}_L(W(t))$ (figure 1*e*) and standard deviation $\sigma_{\mathcal{T}_L(W(t))}$ obtained from the N independent samples of the log-transformed intensity time series $\mathcal{T}_L(W_j(t)) = 10\log(W_j(t)/I_{\text{ref}})$ dB re I_{ref}. Here, the reference intensity is chosen to be $I_{\text{ref}} = P_{\text{ref}}^2/(\rho_a c_a)$, where $P_{\text{ref}} = 20\,\mu$Pa is the standard reference pressure for air, which has density ρ_a and sound speed c_a. This leads to log-transformed intensity $\mathcal{T}_L(W_j(t)) = 10\log|P_j(t)/P_{\text{ref}}|^2$ dB re 20 μPa being expressible in standard sound pressure level (SPL) units for air. We will use the base ten logarithm, log, consistently in log-transformations rather than the natural logarithm, ln, so that theory is more immediately connected to the decibels units typically used in practice.

To more quantitatively delineate the functional dependence of the signal-dependent intensity fluctuations, the mean $\bar{W}(t)$ and standard deviation $\sigma_W(t)$ across temporal pixels t are sorted to obtain standard deviation $\sigma_W(\bar{W})$ as a function of mean intensity $\bar{W}$ in figure 1*f*. The standard deviation is approximately linear in mean intensity with a slope equal to what we define as the scintillation factor, which is the square root of the scintillation index [18,20]. After similar sorting of the corresponding log-transformed intensity statistics (figure 1*g*), the standard deviation in this case $\sigma_{\mathcal{T}_L(W)}$ is more clearly seen to be a constant function of the mean $\overline{\mathcal{T}}_L(W(t))$. The noise is signal-independent after log-transformation of the intensity data. Log-transformation then behaves as a variance-stabilizing transformation.

A general variance-stabilizing transform can be expressed as [23,24]

$$\mathcal{T}_V(I) = \alpha_0 \int_{I_0}^{I} \frac{1}{\sigma_I(\bar{I})}\,\mathrm{d}\bar{I} + \beta_0, \tag{2.1}$$

for random variable I with mean $\bar{I}$ and standard deviation σ_I that depends on this mean. The variance-stabilizing transformed random variable $\mathcal{T}_V(I)$ has a standard deviation $\sigma_{\mathcal{T}_V}$ that is independent of either mean $\overline{\mathcal{T}}_V(I)$ or $\bar{I}$, where I_0 is the minimum value of I, and α_0 and β_0 are arbitrary constants.

To quantitatively compare the effect of log versus variance-stabilizing transformation, the variance-stabilizing transformation of equation (2.1) with $I = W$ is applied to each random sample of the entire rustling leaves intensity time series leading to $\mathcal{T}_V(W_j(t))$ for $j = 1, 2, 3, \ldots, N$, where $\sigma_I(\bar{I}) = \sigma_W(\bar{W})$ is obtained from the acoustic time series data of figure 1*f*. The constants α_0 and β_0 are chosen such that $\mathcal{T}_V(W)|_{\mathcal{T}_L(W)=0\text{ dB re }20\,\mu\text{Pa}} = 0$ and $\mathcal{T}_V(W)|_{\mathcal{T}_L(W)=60\text{ dB re }20\mu\text{Pa}} = 60$ for convenient visual comparison with the log-transformation. The standard deviations $\sigma_{\mathcal{T}_V(W)}$ of the N independent random samples of $\mathcal{T}_V(W_j(t))$ are practically identical to those of log-transformed intensity, as seen in figure 1*g*. The nearly identical dependence of log-transformation and variance-stabilizing transformation on mean intensity for the natural sound intensity fluctuations measured is shown in figure 1*h*. The results of figure 1*a–h* are consistently found for the other natural acoustic events investigated (electronic supplementary material, figure S1).

In addition to log and variance-stabilizing transformations, transformations developed specifically for psychophysics, such as Fechner's, are also shown in figure 1*h* as a function of mean sound intensity. Fechnerian transformation of an external stimulus $\bar{I}$ [29,54,55] can be expressed analytically in terms of measured just-noticeable-differences $\Delta I_i(\bar{I})$ of that stimulus, via [6,27,28]

$$\mathcal{T}_F(I) = \int_{I_0}^{I} \frac{1}{\Delta I(\bar{I})}\mathrm{d}\bar{I}, \tag{2.2}$$

where I_0 is the minimum value of the stimulus. The Fechnerian transformation of figure 1*h* is obtained by applying equation (2.2) to the just-noticeable-difference data of figure 2*a*,*b*. Specifically, the dependencies $\Delta W(\bar{W})$ from eight independent psychophysical experiments [2–6,49] transmitting random broadband sound are used to yield corresponding Fechnerian transformed intensity curves via equation (2.2), with acoustic intensity W substituted for the generic stimulus I, the mean of which is shown in figure 1*h*. This mean curve is linearly scaled and offset for comparison with other transforms in figure 1*h*. Only historic measurements of $\Delta W(\bar{W})$ are used that: (i) employ broadband transmission stimuli filling the entire roughly 128 Hz critical

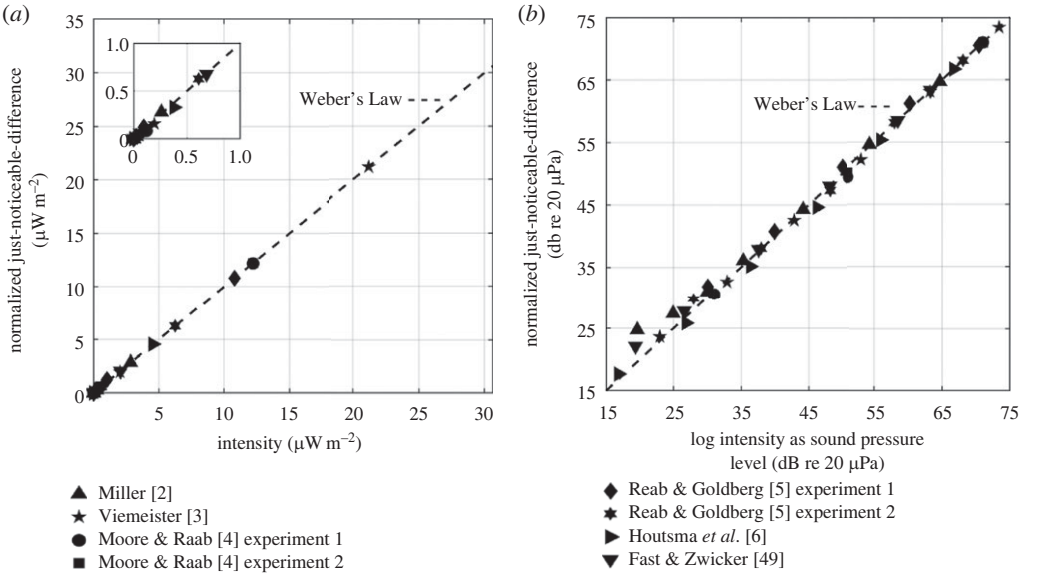

Figure 2. Just-noticeable-differences in acoustic intensity approximately follow Weber's Law. (*a*) Just-noticeable-differences as a function of acoustic intensity stimulus from artificial sound sources obtained from decades of psychophysical experiments measuring human response to sound with broad spectra filling the entire 128 Hz critical band centred at 1000 Hz [2–6,49]. Just-noticeable-differences from each independent experiment display excellent fit to a straight line and consequently Weber's Law. The independent experiments employed acoustic signal stimuli of differing duration and different human subjects which lead to best-fit lines with differing slopes across experiments. Best-fit slopes are normalized to the same value to visually compare linearity of just-noticeable-differences versus stimulating intensity across experiments (electronic supplementary material, table S1). Data shown roughly 10 dB above absolute lowest detectable sound pressure level to avoid contamination from auditory system self-noise or ambient noise contamination. Inset image zooms in on lower intensities. (*b*) Same values as plotted in (*a*) but in decibels as a function of stimulating sound pressure level.

band [54] at 1 kHz of our acoustic measurements and (ii) cover the range of our acoustic intensity data from 15 to 75 dB re 20 μPa. This is done for comparison with our experimental data of natural sound scintillation. We chose the 1 kHz critical band for our measurements because 1 kHz is the frequency at which the minimum audible SPL is defined for humans and it also falls at the lower end of the most sensitive frequency range in human hearing [56].

Fechnerian, log and variance-stabilizing transformations have nearly identical dependencies (figure 1*h*). These observations are quantitatively confirmed in figure 1*i* by comparing normalized correlation coefficients [30] for functional dependencies shown in figure 1*h*.

Interestingly, in decades of previous human psychophysical experiments with controlled artificial sound sources, just-noticeable-differences were found to grow approximately in proportion to stimulating sound intensity. These just-noticeable-differences approximately follow Weber's Law, as seen in figure 2. They do so over the same ranges as our scintillating intensity data from natural sound sources, which have an intensity standard deviation that also follows Weber's Law, as seen in figure 1*f*.

Similar results are obtained for other critical frequency bands (electronic supplementary material, figure S2) and higher intensities (electronic supplementary material, figure S3).

Psychophysical magnitude estimation experiments [54,57,58] lead to a dependence on mean intensity stimulus quite different from log and variance-stabilizing transformation that is somewhere in between those and the direct dependence mean intensity has on itself as shown in figure 1*h–i*. In magnitude estimation, a subject detects a change in intensity stimulus and then makes a judgement to assign a numerical value for the appraised magnitude of the

change. This involves a further intellectual process beyond detecting a change or just-noticeable-difference [55] which may account for its significant departure from the highly correlated log, variance-stabilizing and Fechnerian transformation dependencies (figure 1*h*,*i*). The empirical magnitude estimation transforms used in figure 1*h*,*i* are the average of five independent historic psychophysical experiments measuring human response to sound, including the entire 128 Hz critical band centred at 1000 Hz [2,50–52]. This average curve is linearly scaled in figure 1*i* for comparison with other transformations of intensity. Only historic measurements that roughly cover the range of our acoustic intensity data from 15 to 75 dB are used.

3. Naturally scintillating daylight luminance

We conducted a series of experiments to investigate the natural scintillation of typical objects found in forest or meadow settings illuminated by daylight. Static scenes of natural objects including leaves, feathers, branches, earth, tree bark and stones were imaged every second over daylight hours (figure 3*a*). This was done to form different observations of the same scene changed at each pixel only by variations in natural lighting, which scintillated under varying atmospheric and cloud conditions. Statistical fluctuations of natural light at each pixel in respective intensity images were obtained in this way. The temporal, spatial and frequency samplings were selected to be consistent with those found for the human visual systems.

The static luminance scene of various natural objects in figure 3*a* was imaged with naturally scintillating daylight using a Phantom UHS12 camera. It provided 12 bit depth leading to 4096 discrete luminance values at each pixel in a 1280 by 800 pixel image. The angular resolution of each pixel was approximately 1 arc-min, similar to that of the human eye [61]. The entire scene was measured every second over two and a half hours at midday in Massachusetts under partly sunny sky conditions with 51–69% varying cloud cover leading to $N = 9000$ sample images of the entire scene. Measured luminance $\mathcal{L}_j(x, y)$ at pixel (x, y) for the jth entire-scene sample is proportional to intensity (electronic supplementary material), and has corresponding log-transformed luminance $\mathcal{T}_L(\mathcal{L}_j(x, y)) = 10 \log(\mathcal{L}_j(x, y)/\mathcal{L}_{\text{ref}})$ dB re $\mathcal{L}_{\text{ref}} = 1\,\mu\text{candela m}^{-2}$. Variance-stabilizing transformed luminance is $\mathcal{T}_V(\mathcal{L}_j(x, y))$ from equation (2.1) using our measured luminance data. Fechnerian transformed luminance is $\mathcal{T}_F(\mathcal{L}_j(x, y))$ from equation (2.2), and magnitude estimation transformed luminance is $\mathcal{T}_{\text{ME}}(\mathcal{L}_j(x, y))$ using psychophysical data to be described.

The sample mean $\bar{\mathcal{L}}(x, y)$ and standard deviation $\sigma_{\mathcal{L}}(x, y)$ at any pixel across all $j = 1, 2, 3, \ldots, N$ samples of the entire scene are computed. These are then sorted across pixels (x, y) to obtain the standard deviation as a function of mean luminance $\sigma_{\mathcal{L}}(\bar{\mathcal{L}})$ in figure 3*b*. The standard deviation is found to have an approximately linear dependence on the mean, indicating signal-dependent noise, with slope of approximately 0.21 equal to the scintillation factor.

The Fechnerian transformations of figure 3*d*–*e* are obtained by inserting into equation (2.2) just-noticeable-difference measurement sets $\Delta\mathcal{L}$ from four independent psychophysical experiments [7–9,12], which cover the luminance range of our environmental measurements (figure 4). A linear scaling and offset of the Fechnerian transform dependence is applied to enable visual comparison with other transforms in figure 3*d*. Below the range of our environmental data but above the operational range of low-light-level rod cells [60], i.e. roughly luminance $\mathcal{L} > 1$ candela m^{-2}, Fechnerian transformation maintains a high average correlation, 0.98 normalized correlation coefficient, with log-transformed luminance. To obtain the magnitude estimation transform of figure 3*d*–*e*, only historic psychophysical experiments over the range of our optical luminance data [57,59] are used.

The standard deviations versus mean of log-transformed and variance-stabilizing transformed luminance are shown in figure 3*c*. They have nearly identical constant dependencies on their respective means, indicating that signal-dependent noise in luminance is converted to signal-independent noise by both the log and variance-stabilizing transformations. The functional dependence of log, variance-stabilizing and Fechnerian transformations are seen to be nearly identical, while those for magnitude estimation and untransformed luminance differ significantly from these and each other (figure 3*d*). This is quantitatively confirmed by the correlations between

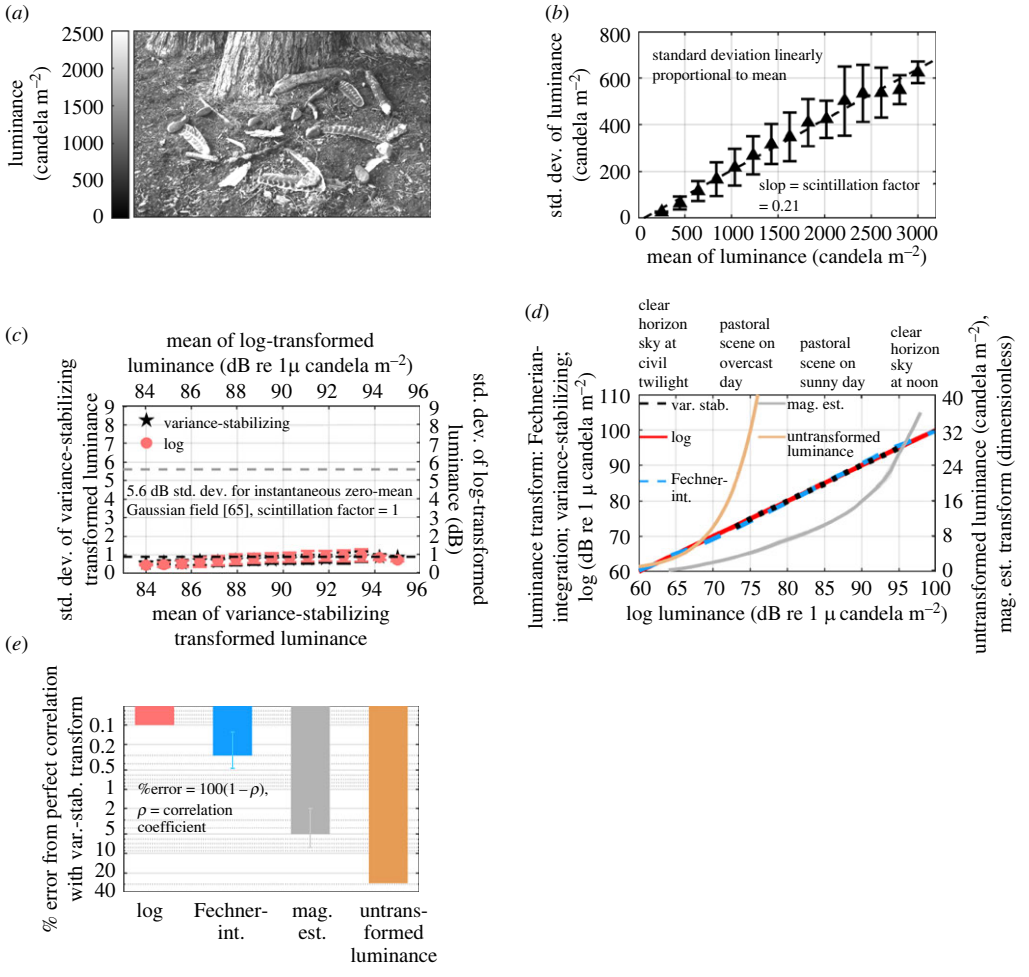

Figure 3. A scene with natural objects illuminated in terrestrial daylight is repeatedly measured to determine the statistical properties natural luminance scintillation at every spatial pixel. Luminance is spectrally filtered, normalized intensity (electronic supplementary material). (*a*) Single measurement sample of scene with static natural objects at 1 arc-min resolution per pixel approximately that of human eye. (*b–e*) Analysis of scene scintillation measured in 51–69% varying cloud cover at 1 s sampling: (*b*) Standard deviation linear in mean for luminance. (*c*) Standard deviation constant function of mean for variance-stabilizing and log-transformed luminance. (*d-e*) Same as figure 1*h–i* except for luminance data of figure 2*a* scene, variance-stabilizing transform is obtained from the measured luminance data, Fechnerian and magnitude estimation transform derived from decades of independent psychophysical investigations [7–9,12,57,59], for data in the daylight range, above the low-light level rod cell range [60]. Similar results are found under different cloud conditions (electronic supplementary material, figures S5 and S7) and for individual objects in the scene (electronic supplementary material, figure S4).

the functional dependencies of the various luminance transforms shown in figure 3*e*. The nearly continuous mean luminance levels $\bar{\mathcal{L}}$ and mean transformed luminance levels from the data are uniformly sampled at discrete points for presentation purposes only in figure 3*b,c*. Again these results (figure 3*a–c*) are for partly cloudy conditions, with similar results obtained for sunny (electronic supplementary material, figure S5) and overcast (electronic supplementary material, figure S7) cloud conditions. The variance-stabilizing transform curve $\mathcal{T}_V(\mathcal{L})$ in figure 3*d* is obtained by concatenating or averaging curves obtained from these three days of distinct cloud conditions.

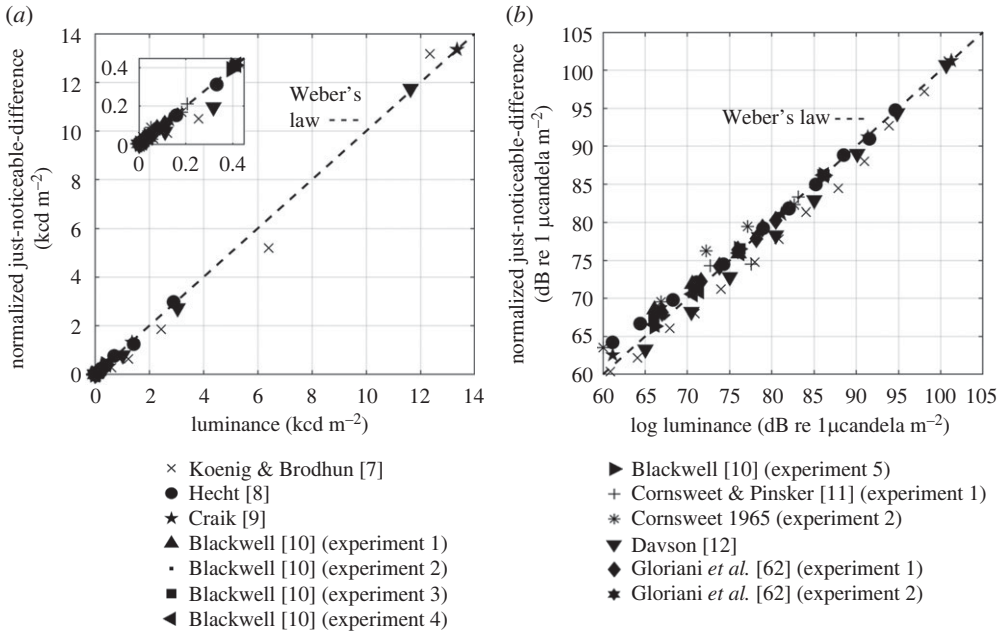

Figure 4. (*a*) Just-noticeable-differences as a function of luminance stimulus from artificial light sources obtained by decades of psychophysical experiments [7–12,62] over the daylight range. Just-noticeable-differences from each independent experiment display excellent fit to a straight line and consequently Weber's Law. The independent experiments employed differing stimulating luminance-patch angular widths, and different human subjects, which lead to differing best-fit slopes across experiments. Best-fit slopes are normalized to the same value to visually compare linearity of just-noticeable-differences versus stimulating luminance across experiments (electronic supplementary material, table S2). Inset image zooms in on lower intensities. (*b*) Same values as plotted in (*a*) but in decibels as a function of log-transformed luminance in decibels.

Empirical just-noticeable-differences in luminance from decades of psychophysical experiments (figure 4*a*,*b*) show an approximately linear dependence on mean stimulating luminance from a controlled artificial light source. They approximately follow Weber's Law as seen in figure 4*a*,*b*. Natural objects illuminated by scintillating daylight in our data have a luminance standard deviation that also follows Weber's Law as seen in figure 3*b*. This leads to the observed high correlation between log-transformed, variance-stabilizing transformed and Fechnerian transformed luminance in figure 3*c*–*e*.

4. Theoretical proof of when Fechner's transformation is a variance-stabilizing transformation

It is now straightforward to mathematically prove that when Weber's Law holds for psychophysical just-noticeable-differences, and stimulating intensity and luminance have standard deviations that grow in direct proportion to their respective means, the Fechnerian transformation is identical to a variance-stabilizing transformation. The fact that both are identical to a log-transform in this case will be seen to follow immediately.

More generally, by the definitions of the Fechnerian transformation $\mathcal{T}_F(I)$ of equation (2.2) and the variance-stabilizing transformation $\mathcal{T}_V(I)$ of equation (2.1) it follows that

$$\mathcal{T}_V(I) = \mathcal{T}_F(I), \tag{4.1}$$

when

$$\sigma_I(\bar{I}) = \alpha_0 \Delta I(\bar{I}), \tag{4.2}$$

where the arbitrary offset β_o of the variance stabilization equation (2.1) is set to zero, and linear dependence of $\sigma_I(\bar{I})$ and $\alpha_0 \Delta I(\bar{I})$ on $\bar{I}$, as in Weber's Law, is just one of many mathematically possible ways for the equalities to hold.

The equality of equation (4.1) has been experimentally demonstrated here in figure 1*h–i* for acoustic intensity data and figure 1*d–e* for optical luminance data. The equality of equation (4.2) is also experimentally verified here by comparison of figures 1*f* and 2*a,b* for the acoustic intensity data and figures 3*b* and 4*a,b* for the optical luminance data.

For constant scintillation factor

$$s = \frac{\sigma_I(\bar{I})}{\bar{I}}, \tag{4.3}$$

as seen for measured intensity and luminance in figures 1*f* and 3*b*, equations (4.1)–(4.3) lead to the variance-stabilized solution for Fechnerian transformed intensity

$$\mathcal{T}_F(I) = \frac{\alpha_0}{s} \frac{10 \log(I)}{10 \ln(e)} + \gamma_0, \tag{4.4}$$

which is a logarithmic transform of received intensity stimulus, consistent with the corresponding measured dependencies in figures 1*h* and 2*d*, where, like α_0 and s, γ_0 is also a constant. This also explains the high correlation found between log, variance-stabilizing and Fechnerian transformed intensity and luminance in figures 1*g–i* and 3*c–e*, respectively. Arriving at equation (4.4) from the Fechnerian transformation of equation (2.2) with just-noticeable-differences obeying Weber's Law is a well-known result in psychophysics, namely derivation of the Weber–Fechner Law [1,6,27–29]. Arriving at equation (4.4) from variance-stabilizing transformation of scintillating sound and light intensity data (equation (2.1)), however, puts the Weber–Fechner Law in a new context. It shows that perception in log-transformed intensity or luminance is tantamount to having perception in a variable that has a constant standard deviation, i.e. a constant statistical resolution scale, with respect to the external stimuli. The external stimuli in this case are the log-transformed intensity and luminance of naturally scintillating sound and light, respectively.

5. Approximate normality of variance-stabilizing-transformed intensity or luminance

The Kolmogorov–Smirnov (K–S) test for Gaussianity [63,64] is applied to each temporal pixel in the acoustic rustling leaves event of figure 1 and each spatial pixel in the natural scene illuminated by daylight of figure 3 across independent samples of each. The percentage of pixels that pass the K–S test at 5% significance level is shown in figure 5*a,b* for acoustic and daylight cases, respectively. Results for the various transforms of intensity and luminance, as well as untransformed intensity and luminance are also shown in figure 5 for comparison.

Variance-stabilizing, Fechnerian and log-transforms of intensity and luminance lead to effectively normal probability densities for the vast majority of pixels as quantified by K–S testing (figure 5*a,b*). The fit to normality is consistently cruder for magnitude estimation and consistently worst for no intensity or luminance transformation (figure 5*a,b*). This hierarchy is identical to that found in correlation with the variance-stabilizing transform (figures 1*i* and 3*e*). Variance-stabilizing transformations have been correlated with transformations to normality [24,25]. This is apparently due to more rapid convergence by the central limit theorem for random variates that are more similarly distributed.

Transformation to a normal random variable has practical benefits, because it entails complete characterization of the random variable's probability density by its first two moments. The fact that log-transformation of the natural intensities and luminances measured here leads to effectively normally distributed data is fortuitous for this reason and another. In the random generation, propagation and scattering of waves, lognormal intensity and luminance distributions are converged upon from a number of diverse mechanisms via the central limit theorem. This makes them predictable, which makes adaptation to them more effective and reliable.

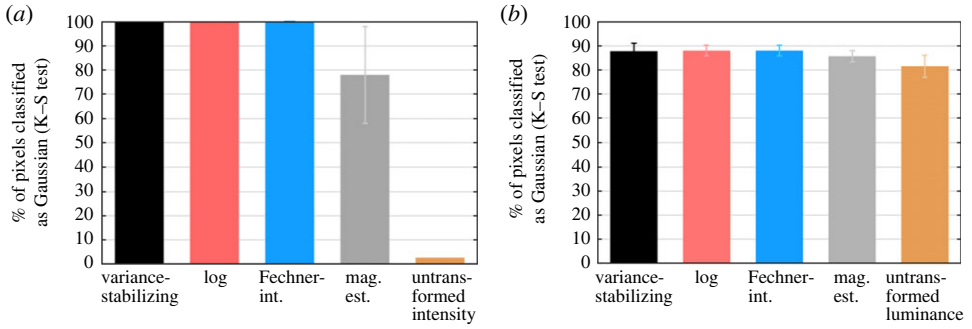

Figure 5. Percentage of normally distributed image pixels by Kolmogorov–Smirnoff (K–S) test for (*a*) the $N = 154$ samples of the entire acoustic intensity time series of the rustling leaves event of figure 1, (*b*) and the $N = 9000$ samples of the daylight luminance scene of figure 3. The K–S test is also performed for various transformations of intensity in (*a*) and various transformations of luminance in (*b*). Similar results are obtained for other examples in the electronic supplementary material.

As Rayleigh explained [22], natural sounds are often a superposition of many additive pressure waves from independent random source components that converge to a zero mean Gaussian field by the Central Limit theorem. The intensity of such a random field has a standard deviation proportional to mean intensity which is in turn proportional to the wave field variance [65]. Following the homomorphic properties of log-transformation, log-transformed intensity at any pixel then has a standard deviation independent of the signal-bearing mean, and tends towards normality [65,66]. This is consistent with measurements shown in figures 1 and 5*a*. The standard deviation of log-transformed intensity in decibels (figure 1*g*) is slightly lower than that of an instantaneous Gaussian random field data, which is 5.6 dB [65]. It is consistent with roughly two statistically independent coherence cells averaged per pixel for the given temporal and spectral windowing rather than a single one for the instantaneous case [65]. Convergence to a lognormal intensity probability density could also be hastened by multiple random and independent factors affecting the acoustic signal received, such as source power and range, which become additive after log-transformation.

Lognormal intensity scintillation is also routinely observed in light after propagation through the atmosphere. This has been well documented in starlight twinkling [19,20] and sunlight scintillation due to random atmospheric effects [21,67,68]. The natural scintillation of terrestrial daylight we observe at any pixel in our luminance images (figure 3*b*,*c*) arises from sunlight scattering through and from multiple random and independent atmospheric layers [19–21,67,68], including clouds, and subsequent directional scattering by the object into a directional sensor such as the eye. Log-transformation of this light intensity or luminance homomorphically converts random independent multiplicative factors to additive ones [18,20]. This leads to a log-intensity standard deviation that is independent of the signal-bearing mean (figure 3*c*) as well as convergence to a lognormal intensity probability density by the central limit theorem [18,20,26]. A small fraction of pixel locations are not classified as having normal densities in the better performing transformations of figure 5*b* due to variations in shadows cast by some objects and wind-induced motion. These effects typically can be deterministically modelled by practical means, which is often not the case for scintillation from random atmospheric fluctuation.

Adjustment to the average image level across pixels in any instantaneous image has precedent in observed visual system threshold shifting [69] and is accomplished for luminance images and their transforms via

$$\tau_\psi(\mathcal{L}_j(x,y)) = \mathcal{T}_\psi(\mathcal{L}_j(x,y)) - \frac{1}{N_x N_y}\sum_{x=1}^{N_x}\sum_{y=1}^{N_y}\mathcal{T}_\psi(\mathcal{L}_j(x,y)), \tag{5.1}$$

for any transform $\mathcal{T}_\psi$ and instantaneous luminance image sample $\mathcal{L}_j(x,y)$. To account for threshold shifting in the visual system and typical of machine systems, equation (5.1) is applied when specified to each transform of luminance data, including the untransformed luminance used in the tests of normality in figure 5*b*. This linear shift does not affect the image pattern at any sample j of the entire image. For all transforms effective at variance stabilization, application of equation (5.1) leads to (i) greater stability across variations in cloud cover in the standard deviation of transformed luminance as well as (ii) statistical decorrelation between spatially separated pixels. Across all samples of the luminance image of figure 3*a* and all spatial pixels, the standard deviation $\sigma_{\tau_L(\mathcal{L})}$ is 0.378 dB, while without the adjustments of equation (5.1) the standard deviation $\sigma_{T_L(\mathcal{L})}$ is roughly 0.90 dB as shown in figure 3*c*.

The K–S test as applied in figure 5*a*,*b* requires the number of independent observations N_{ind} of the random image used to form the empirical distribution. In the acoustic case, each sample of the entire image is statistically independent and the number of samples of the entire image is $N_{\text{ind}} = N = 154$. For the optical case, the approximate number of independent samples of each pixel, roughly $N_{\text{ind}} = 163$ which is less than the total number of temporally consecutive samples $N = 9000$, is determined from the autocorrelation of $\tau_\psi(\mathcal{L}_j(x,y))$ across temporally consecutive samples j in two ways that yield the same results to within roughly 5%. In one approach the number of independent samples is set equal to the total uninterrupted time over which consecutive samples are measured, roughly 2.5 h, divided by the e-folding time of the autocorrelation [30,70] of the pixel value's temporal dependence, which is found to be roughly 55 s. In the other, the fact that fluctuations of the autocorrelation function at lags far from the zero-lag peak form a normal distribution with zero mean and variance given by the reciprocal of the number of independent observations is used [70]. By finding the root-mean-square level, δ, of the autocorrelation function many time lags away from zero to within a 95% confidence interval, i.e. values within 1.96 times the standard deviation about the mean, the number of independent observations can be computed as $(1.96/\delta)^2$ [70].

6. Weber's Law is a consequence of attaining the Cramer–Rao lower bound in intensity or luminance resolution

Simple analytic equations can now be derived for the Cramer–Rao lower bound [30] on the mean-square error in the estimation of parameters from naturally scintillating sound intensity and light luminance data. No unbiased estimates can have a mean-square error smaller than the Cramer–Rao lower bound [30]. An unbiased estimate is one that has an expectation value that equals the true value of the parameter to be estimated.

For a normal random variable $\mathcal{T}_L(\mathcal{I}) = 10\log(\mathcal{I})$ with mean $\overline{\mathcal{T}}_L(\mathcal{I})$ that depends on the parameter to be estimated θ and variance $\sigma^2_{\mathcal{T}_L(\mathcal{I})}$ that is independent of θ, the Cramer–Rao lower bound for mean-square estimation error of θ is

$$\mathcal{CRLB}(\theta) = \sigma^2_{\mathcal{T}_L(\mathcal{I})}\left(\frac{\mathrm{d}\overline{\mathcal{T}}_L(\mathcal{I})}{\mathrm{d}\theta}\right)^{-2}, \tag{6.1}$$

where

$$\overline{\mathcal{T}}_L(\mathcal{I}) = 10\log\left(\frac{\bar{\mathcal{I}}}{\sqrt{1+s^2}}\right), \tag{6.2}$$

and

$$\sigma_{\mathcal{T}_L(\mathcal{I})} = 10\log(e)\sqrt{\ln(1+s^2)}, \tag{6.3}$$

for lognormal $\mathcal{I}$ and constant scintillation factor s from equation (4.3). In other words, for any unbiased estimate $\hat{\theta}$ of θ from random data $\mathcal{T}_L(\mathcal{I})$, the mean-square estimation error $\langle(\hat{\theta}-\theta)^2\rangle$ cannot be less than $\mathcal{CRLB}(\theta)$ [30]. The measured standard deviations for log-transformed acoustic intensity (figure 1*g*) and log-transformed luminance (figure 3*c*) are indeed found to be equal to those predicted by equation (6.3) upon insertion of the measured scintillation factors s from

figures 1*f* and 3*b*, respectively. This also demonstrates effective lognormality of the observed acoustic intensity and optical luminance data at each pixel.

If the parameter to be estimated is the mean of the lognormal variable, $\theta = \bar{\mathcal{I}}$, the Cramer–Rao lower bound from equations (6.1) and (6.3) leads to the minimum possible root-mean-square error,

$$\sqrt{\mathcal{CRLB}(\bar{\mathcal{I}})} = \frac{\sigma_{\mathcal{T}_L(\mathcal{I})}}{10\log(e)}\bar{\mathcal{I}} = \sqrt{\ln(1+s^2)}\bar{\mathcal{I}}, \tag{6.4}$$

which is directly proportional to $\bar{\mathcal{I}}$ as in Weber's Law. When $\mathcal{I}$ represents the random acoustic intensity W/I_{ref} data at any pixel for the rustling leaf example, which is shown to be approximately lognormally distributed in figure 5*a*, inserting either the scintillation factor shown in figure 1*f* or the constant log-transformed standard deviation of figure 1*g* into equation (6.4) leads to the Cramer–Rao lower bound on mean-square error in estimation of acoustic intensity, $\sqrt{\mathcal{CRLB}(\bar{W})}/\bar{W} = 0.82$, shown in figure 6*a*. We find adjustment to the mean image level across pixels has a negligible effect on normality of the various transforms of the acoustic intensity data, so it is not performed here. Such adjustments, as described in equation (5.1), do make variance-stabilizing transformed luminance more normal at each pixel, and are both well documented in human vision and routinely used in machine vision [69,71]. Along these lines, when $\mathcal{I}$ represents daylight luminance $\mathcal{L}/\mathcal{L}_{\text{ref}}$, which is shown to be approximately lognormally distributed in figure 5*b*, the Cramer–Rao lower bound $\sqrt{\mathcal{CRLB}(\bar{\mathcal{L}})}/\bar{\mathcal{L}} = 0.087$ shown in figure 6*c* is then obtained by use of $\sigma_{\mathcal{T}_L(\mathcal{I})} = \sigma_{\tau_L(\mathcal{L})} = 0.378$ dB in equation (6.4) which includes application of the equation (5.1) instantaneous image shift. Similar results are found for other acoustic event signatures (electronic supplementary material, figure S1) and scenes illuminated under different cloud conditions (electronic supplementary material, figures S5 and S7).

Since varying transmission time durations of the broadband acoustic signals were used to measure just-noticeable-differences in the assorted independent psychophysical experiments [2–6,49], the different psychophysical datasets are normalized to a consistent intensity stimulus time duration in figure 6*a*,*b*. This is taken to be the nominal 10 ms duration of a single auditory system pixel [54]. For this normalization, unnormalized just-noticeable-differences are divided by the square root of the ratio of the applied signal duration to the nominal 10 ms temporal resolution scale to be consistent with empirical observations of the dependence of just-noticeable-differences on signal duration [5]. This dependence is congruous with intensity averaging in a random process [65]. Similarly, to compare just-noticeable-differences across psychophysical experiments that use stimulating luminance patches of varying angular widths ϕ as subtended from the subject's eye, the just-noticeable-differences in figure 6*c*,*d* are normalized to the nominal angular resolution of the eye following empirically derived patch-size dependencies [10,72]. Specifically, normalized just-noticeable-differences are obtained as $\Delta\mathcal{L} = (\phi/\phi_{\text{eye}})^{0.5}\Delta\mathcal{L}_{\text{unnorm}}$ for $\phi \le \phi_{\text{fov}}$, and $\Delta\mathcal{L} = (\phi_{\text{fov}}/\phi_{\text{eye}})^{0.5}\Delta\mathcal{L}_{\text{unnorm}}$ for $\phi > \phi_{\text{fov}}$, where ϕ_{fov} is the roughly 120 arc-min angular span of foveal vision for centre gaze [73], ϕ_{eye} is the roughly 1 arc-min angular resolution of the eye at centre gaze, and $\Delta\mathcal{L}_{\text{unnorm}}$ are unnormalized just-noticeable-differences. Only data from psychophysical experiments where acoustic signal durations and visual patch angular widths are provided are used in figure 6.

Weber's Law is then a consequence of intensity or luminance resolution having the functional dependence dictated by the theoretical Cramer–Rao lower bound. This is seen from equation (6.4) where the theoretical root-mean-square error bound is linearly dependent on mean intensity, $\bar{\mathcal{I}} = \bar{W}/I_{\text{ref}}$, or luminance, $\bar{\mathcal{I}} = \bar{\mathcal{L}}/\mathcal{L}_{\text{ref}}$, so leading to Weber's Law. If interpreted directly as root-mean-square errors, just-noticeable-differences in artificially generated sound intensity $\Delta W(\bar{W})$ and artificial light luminance $\Delta\mathcal{L}(\bar{\mathcal{L}})$ measured during many independent psychophysical experiments are found to approximately attain the respective Cramer–Rao lower bounds of equation (6.4) (figure 6*a*,*c*). This is remarkable because the bounds are determined independently from measurements of naturally scintillating environmental sound intensity and daylight luminance. The just-noticeable-differences follow the same linear dependence as the root-mean-square error bound on mean sound intensity and light luminance. The average of

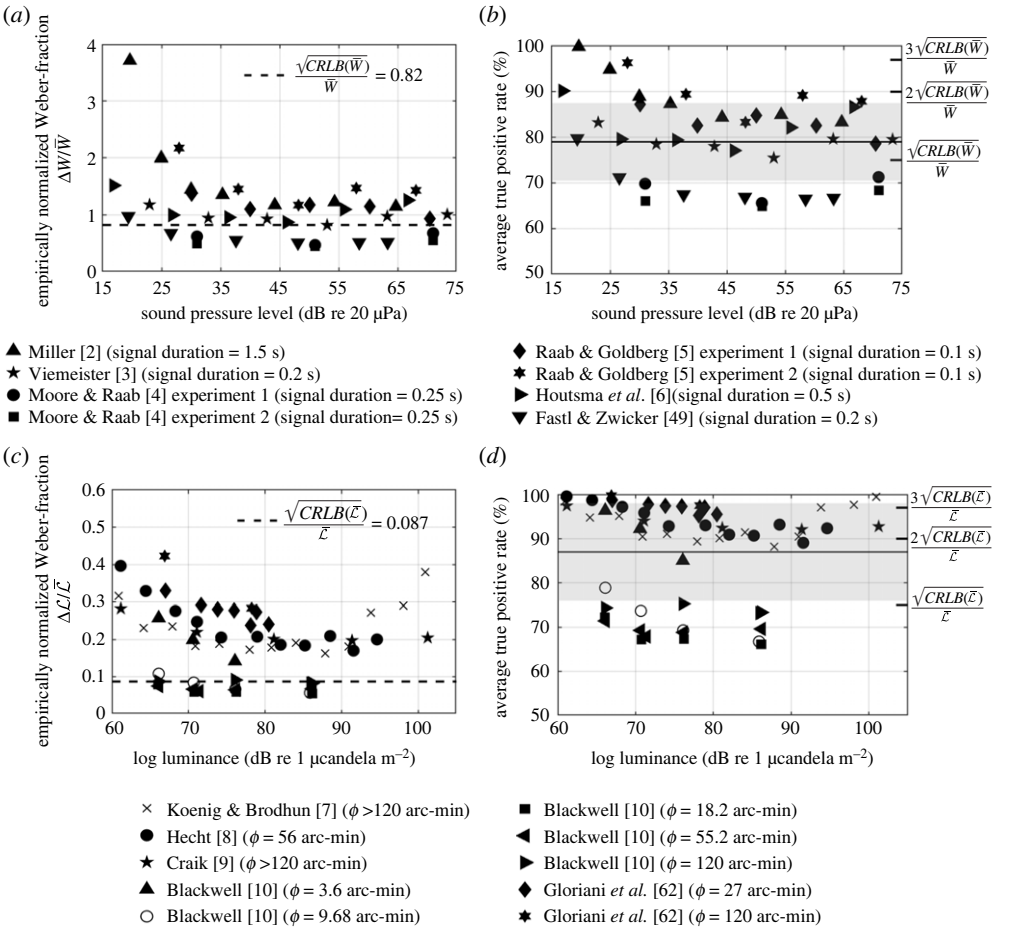

Figure 6. Psychophysical measurements of just-noticeable-differences in sound intensity and light luminance from artificial sources approximately attain the Cramer–Rao bound for natural sound and light scintillation. True positive detection rates for intensity or luminance change using psychophysical just-noticeable-differences as change-detection thresholds are also shown to be in the optimal range for natural scintillating sound and light. Natural sound and light scintillation statistics from figures 1 and 3 datasets are used. (*a*) Ratio of just-noticeable-differences to sound intensity stimulus, known as a Weber fraction, as a function of sound intensity stimulus obtained from decades of psychophysical experiments measuring human response to artificial broadband sound. Artificial sound fills the entire 128 Hz critical band centred at 1000 Hz [2–6,49]. For quantitative comparison, just-noticeable-difference data across independent experiments normalized to a consistent signal transmission duration equal to the nominal 10 ms single pixel temporal resolution of the auditory system. Cramer–Rao lower bound divided by mean intensity stimulus (dashed line) based on measured probability densities of naturally scintillating sound via equation (6.4). (*b*) Average true positive detection rate from natural sound intensity probability density across all false-positive rates for intensity change-detection threshold equal to psychophysically measured just-noticeable-differences for each dataset shown. (*c–d*) Same as (*a–b*) except just-noticeable-differences obtained from decades of psychophysical experiments measuring human response to light luminance stimulus [7–12,62], and probability densities and Cramer–Rao lower bound of equation (6.4) determined from measured scintillation of natural light after the instantaneous mean image shift of equation (5.1). For quantitative comparison, just-noticeable-difference data across independent experiments are normalized to a consistent stimulating signal patch-size spanning the nominal 1 arc-min single pixel angular resolution of the visual system. Similar results are found for other cloud conditions (electronic supplementary material, figures S5 and S7) and sound sources (electronic supplementary material, figure S1).

just-noticeable-differences across many different experimental studies approximately equals the root-mean-square error bound for acoustic intensity. For light luminance, some just-noticeable-difference datasets attain the bound, but the average across datasets is higher than the bound by roughly a factor of two. This is advantageous when the just-noticeable-differences are interpreted as thresholds for change detection rather than directly as root-mean-square errors.

From this perspective, let us consider the just-noticeable-differences as intensity or luminance change-detection thresholds. Let us also consider the performance of integer factors of the respective Cramer–Rao lower bounds on root-mean-square error as change-detection thresholds. Binary hypothesis testing is employed. The probability densities for log-transformed sound intensity and light luminance are then determined for each hypothesis using measured data, summarized in figures 1 and 3, where only the log-transformed variable's mean is different in each hypothesis. This mean includes an intensity or luminance threshold shift in one hypothesis, while in the other no threshold shift is used. Neyman–Pearson hypothesis testing is employed. It yields the highest probability of true positive detection for a given probability of false alarm [37]. As thresholds for detectable change, the just-noticeable-differences measured psychophysically with artificial light and sound sources shown in figure 6*a*,*c* yield average true positive change-detection rates over all false-positive rates of $79 \pm 8.5\%$ for natural sound intensity (figure 6*b*) and $87 \pm 11\%$ for daylight luminance (figure 6*d*) over all false-positive values. They do so relatively consistently for all mean intensities and luminance values. This is a consequence of Weber's Law in both the psychophysical just-noticeable-difference data and the standard deviations of the environmental sound intensity and light luminance data. When the root-mean-square bound is instead used as a threshold for change, the average true positive detection rates are 75% for both acoustic intensity and light luminance. So as a change-detection threshold, the Cramer–Rao lower bound on root-mean-square sound error is on average within 4% for mean sound intensity and 12% for mean daylight luminance of the performance of the respective psychophysical just-noticeable-differences (figure 6). As thresholds for change detection, the psychophysical just-noticeable-differences are then extremely efficient. They are remarkably in the optimal range of being large enough to reject most of the false alarms from natural sound and light scintillation, but not be so large as to also reject changes that are very likely true positive. If, for argument's sake, instantaneous adjustment to the mean luminance across pixels as in equation (5.1) is not performed, despite evidence to the contrary in human perception [69], the root-mean-square luminance Cramer–Rao lower bound becomes approximately 0.21, by use of $s = 0.21$ from figure 3*b* in equation (6.4). As a detection threshold this is within 2% of the average true positive detection performance of just-noticeable-differences in luminance, and so is also in the optimal range.

The Cramer–Rao lower bound in resolving the mean is exactly equal to the variance for log-transformed intensity or luminance. The same is true for variance-stabilizing transformed and Fechnerian transformed intensity or luminance. This is because all of these transformed intensities or luminances can be described by a normal random variable $\mathcal{T}_L(\mathcal{I})$ with standard deviation $\sigma_{\mathcal{T}_L(\mathcal{I})}$ independent of the mean $\overline{\mathcal{T}}_L(\mathcal{I})$, where Weber's Law holds for $\mathcal{I}$ as in equations (6.3) through (6.4) by constancy of s. This leads to

$$\sqrt{\mathcal{CRLB}(\overline{\mathcal{T}}_L(\mathcal{I}))} = \sigma_{\mathcal{T}_L(\mathcal{I})}, \tag{6.5}$$

where it is explicitly seen that the root-mean-square error bound on estimation of the transformed variable's mean is exactly equal to its standard deviation, which is constant and independent of $\bar{\mathcal{I}}$ and $\overline{\mathcal{T}}_L(\mathcal{I})$. Statistically optimal resolution of log-transformed intensity or luminance is then constant. Perception with log-transformed intensity or luminance then conveniently requires optimal resolution of the perceived variate to be invariant to changes in the mean of this variate from equation (6.5). It also leads to Weber's Law for optimal intensity or luminance resolution by equation (6.4). The same is true for variance-stabilizing and Fechnerian transformations of intensity or luminance.

7. Maximizing information reception and optimizing pattern recognition

Intensity perception obeying Weber's Law is found to have a number of other advantages given the natural fluctuations of environmental light and sound intensity. It enables information reception to be easily maximized and pattern recognition easily optimized according to criteria from information, estimation and detection theories [30,35–37]. To see this, let $\mathbf{G}_j$ be an n-dimensional vector of transformed or untransformed scintillating acoustic intensity or daylight luminance data over the n pixels and jth sample of this image. Let the mean of $\mathbf{G}_j$ over all samples j be $\bar{\mathbf{G}}$ and the covariance be C. For two-dimensional transformed or untransformed luminance image data, $\mathbf{G}_j$ is a vectorized form including the values at all spatial pixels, with instantaneous offset adjustment via equation (5.1). Variance-stabilizing, log and Fechner transformed sound intensity and light luminance images $\mathbf{G}_j$ are found to undergo effectively normal fluctuations at each pixel (figure 5). They are also found to have a covariance matrix that is well approximated by $C = \sigma^2\mathrm{I}$, where I is the identity matrix and σ^2 is a variance independent of the mean $\bar{\mathbf{G}}$. In this case, the standard multivariate Gaussian log-likelihood function [30] is appropriate, and can be expressed as

$$l(\bar{\mathbf{G}}, \sigma^2) = \sum_{j=1}^{N} \left\{ -\frac{1}{2} \frac{(\mathbf{G}_j - \bar{\mathbf{G}})^T (\mathbf{G}_j - \bar{\mathbf{G}})}{\sigma^2} \right\} + d, \tag{7.1}$$

where $d = -N(n/2)(\log(\sigma^2) + \log(2\pi))$ is a constant, and the signal-independent variance σ^2 is obtained via maximum-likelihood estimation from image data $\mathbf{G}_j$ for $j = 1, 2, \ldots, N$. For example, $\sigma = \sigma_{\mathcal{T}_L(\mathrm{W})} = 3.87$ dB for log-transformed intensity of the rustling leaves data (figure 1), and $\sigma = \sigma_{\tau_L(\mathcal{L})} = 0.378$ dB for log-transformed luminance data of the scene in figure 3 after application of equation (5.1).

The sum of equation (7.1) is a sufficient statistic [30,35,36,74] in that it contains all information in the multivariate data about the mean image $\bar{\mathbf{G}}$ despite being a scalar variate. For estimation of parameters of the mean image, including recognition of patterns in the image, it is customary to expand the summation into three terms. What we will call the first term is a known scalar constant of the measurement that does not vary with parameters of the mean to be estimated

$$\sum_{j=1}^{N} \left\{ -\frac{1}{2} \mathbf{G}_j^T \mathbf{G}_j \right\}. \tag{7.2}$$

It is proportional to the average squared value at any pixel across all samples of the image. What we will call the second term

$$\left\{ -\frac{N}{2} \bar{\mathbf{G}}^T \bar{\mathbf{G}} \right\}, \tag{7.3}$$

is a scalar parameter either known or to be estimated. The third term

$$\mathcal{Q} = \sum_{j=1}^{N} \left\{ \bar{\mathbf{G}}^T \mathbf{G}_j \right\}, \tag{7.4}$$

is the matched-filter correlation between the mean image and a measurement of it

$$M_j = \mathbf{G}_j^T \bar{\mathbf{G}}, \tag{7.5}$$

summed over all samples of the entire image. If the second term is known, the third term is a sufficient statistic. Typically, the measured and known first term is a very good approximation to the second term, in which case the second term is approximately known. Then the third term is to very good approximation a scalar sufficient statistic containing all information in the multivariate image data about the environmental patterns to be recognized and parameters to be estimated. The environmental signal patterns or parameters that maximize this matched-filter correlation term (equation (7.4)) then also maximize the likelihood function (equation (7.1)) and are maximum-likelihood estimates. The maximum-likelihood estimate has a useful optimality property. If some estimate can attain the lowest possible mean-square estimation error given by

the Cramer–Rao lower bound for sufficiently large N, it must be the maximum likelihood estimate [30,35,74].

Optimal pattern recognition in the sense of maximizing the likelihood function then requires only a very intuitive process. Find the template image mean $\bar{\mathbf{G}}$ that has the best correlation with the measured image on average over measurements of the image. The process could be as simple as trial and error across hypothetical templates in memory. Knowledge of statistical moments higher than the first, corresponding to the mean signal pattern, is not necessary. The key point is that this simple intuitive correlation process is only optimal after the naturally scintillating measurements of sound intensity or light luminance undergo log, variance-stabilizing or Fechnerian transformation. This is because the simple matched filter (equations (7.4) and (7.5)) cancels fluctuations at each pixel. If the fluctuations are signal-independent, as is the case after transformations that stabilize the variance, signal information is not lost by the cancellation. If the fluctuations are signal-dependent, as they are for sound intensity and light luminance before such transformation, the cancellation destroys signal information. Destruction of signal information is not optimal for parameter estimation and does not lead to a sufficient statistic.

Detection of a pattern in image data can also be posed in terms of an optimal way of choosing between two competing hypotheses for the mean image pattern $\bar{\mathbf{G}}_0$ and $\bar{\mathbf{G}}_1$. To maximize the true positive detection probability for a given false positive detection rate is quite straightforward for the Gaussian likelihood function of equation (7.1). The approach, following Neyman & Pearson [30,36,37,74], is to choose $\bar{\mathbf{G}}_1$, which is the correct mean pattern, over $\bar{\mathbf{G}}_0$, when

$$\mathbf{G}_j^T \bar{\mathbf{G}}_1 - \mathbf{G}_j^T \bar{\mathbf{G}}_0 = M_{1j} - M_{0j} > \beta, \tag{7.6}$$

for a given measurement $\mathbf{G}_j$ of the image, where β is determined from the given false-positive rate [30,36,74]. This optimal decision rule (relation (7.6)) is based on a simple and intuitive sufficient statistic, namely the difference between two matched-filter correlations. Again, knowledge of statistical moments higher than the first is not necessary given the normal likelihood model of equation (7.1).

A measure of the relative consistency of the various transforms of sound intensity and light luminance data with the normal likelihood model of equation (7.1) can be obtained by comparing the maximum likelihoods of each assuming this model. This comparison is shown in figure 7*a* across different acoustic sound types and in figure 8*a* across different objects imaged with daylight. The maximum likelihoods are nearly identical and highest for the highly correlated variance-stabilizing, log and Fechnerian transforms. They are significantly lower for magnitude estimation transformation, and the lowest by far for no transformation of sound intensity or light luminance. This is expected because the transforms with high maximum likelihoods are most effective at variance stabilization and transformation to normality. To make this comparison, the mean of the image $\bar{\mathbf{G}}$ and variance parameter σ^2 are estimated by maximum likelihood over all data samples. This is done for each transform, as well as untransformed intensity or luminance. Since the random image for each transform is in different units, transformation to a common physical image unit is necessary before comparison. This is achieved by standard Jacobian transformation of multivariate probability densities [30].

So, for sound intensity and light luminance images that undergo variance-stabilizing, log or Fechnerian transforms, no higher statistical moments beyond the first need be estimated for statistically optimal pattern recognition. In a hostile or competitive environment this is advantageous because it leads to rapid and efficient pattern recognition. Perception with these transformations is then consistent with advantageous adaptation to the natural scintillation of environmental sound and light.

8. Advantages of sensing with Weber's Law quantified with experimental data

There are a number of ways to elucidate practical advantages of the current findings. One is to consider the consequences if they are not put to use. Suppose, for example, the resolution of a sensing system, which can be taken to correspond to a just-noticeable-difference in human

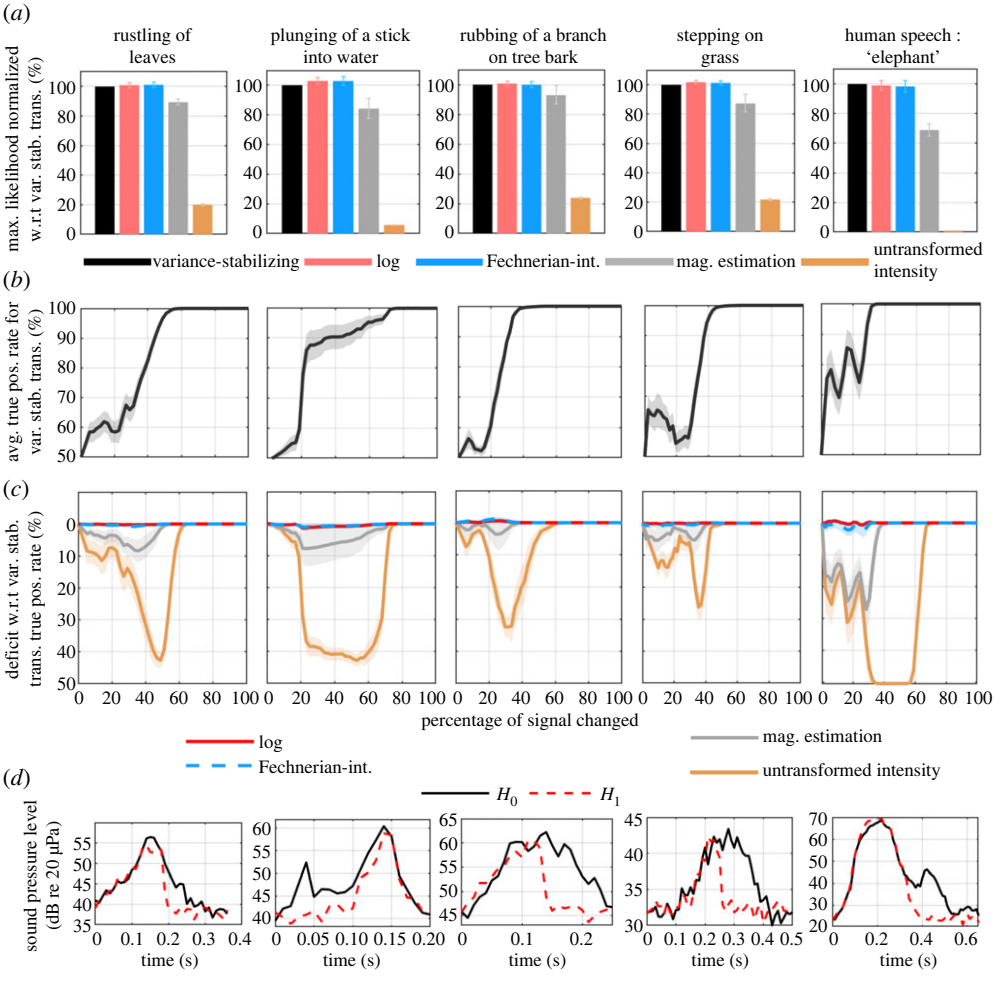

Figure 7. Information reception and pattern recognition performance compared across transformations of natural scintillating acoustic intensity signals for a Gaussian likelihood model with constant variance and no correlation across pixels (equation (7.1)). Perception with log, variance-stabilizing and Fechnerian transformed intensity fits this model well and leads to optimal pattern recognition. Columns span distinct acoustic event signatures in auditory critical band at 1 kHz (1 ± 0.064 kHz) and 10 ms pixel increment. (*a*) Maximum of the likelihood function across transforms with respect to those of variance-stabilizing transformed intensity. (*b–d*) Hypothesis testing between changed image Hypothesis 1 and unchanged image Hypothesis 0 as a function of the number of changed pixels. Changed pixels are replaced with ambient noise at the minimal signal level. (*b*) Average true positive rate across all false-positive rates for variance-stabilizing transformed intensity. Competing hypotheses go from indistinguishable to completely distinguishable as number of pixels changed increases from zero. (*c*) Comparison of detection performance across transforms in per cent deficit from variance-stabilizing performance shown in (*b*). (*d*) Example of sample means from 10 independent samples unchanged data in black, changed data in red for 50% of raw time acoustic pressure series dropped to ambient noise level. All changes progress from time series end except for stick plunging into water where changes progress from beginning.

perception, is constant in acoustic intensity rather than constant in log-transformed intensity. Suppose the repeated measurements of a natural sound event, such as rustling leaves in figure 1, has a scintillation factor of nearly one for any pixel. This leads to a standard deviation approximately equal to mean intensity. Setting system resolution at the highest value of the measured standard deviations, which is found for the greatest mean intensity, would make it impossible to resolve most of the rest of the time series which has much smaller mean levels. In

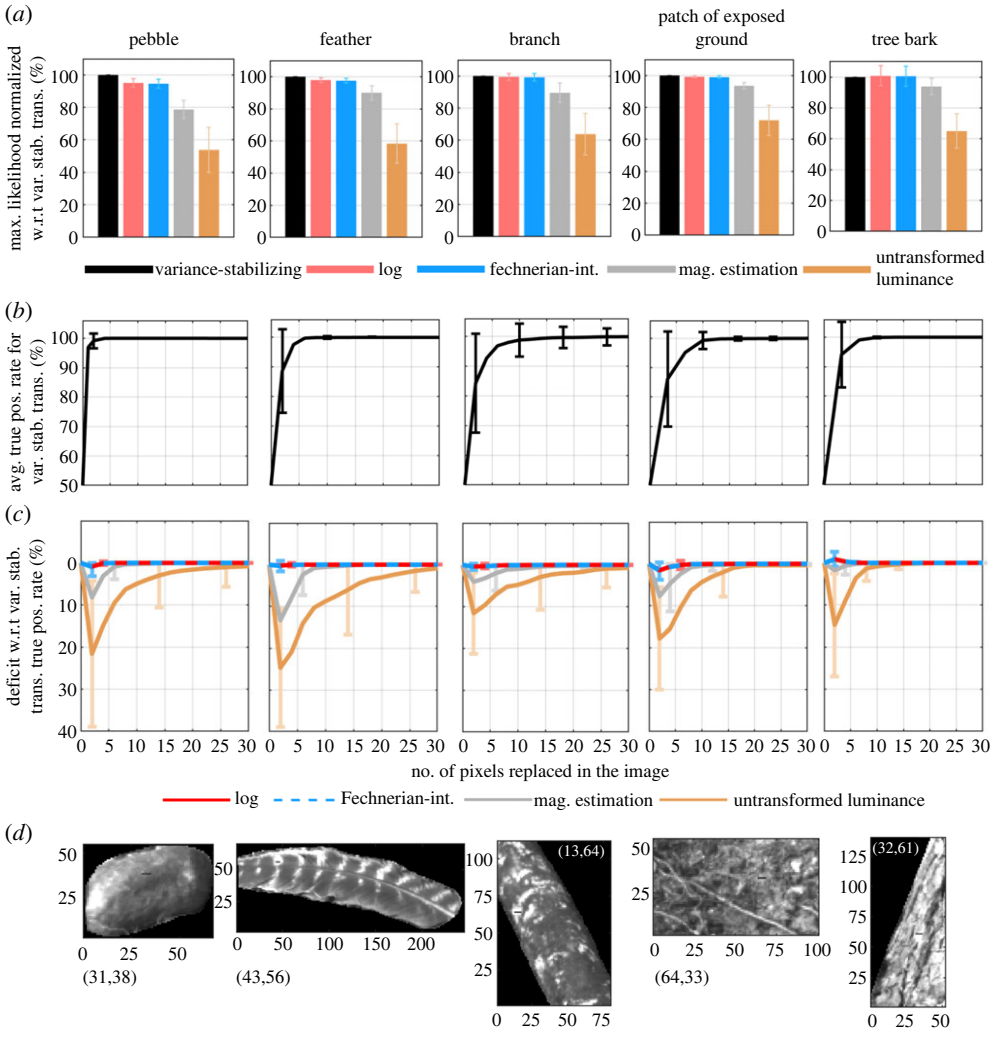

Figure 8. Same as figure 7 except for objects imaged with naturally scintillating daylight from figure 3. Perception with log, variance-stabilizing and Fechnerian transformed luminance leads to optimal pattern recognition. (*a*) Maximum of likelihood function across transforms and objects. (*b–d*) Changed pixels are replaced with low luminance earth or mud pixels. They grow horizontally up to 10 pixels in each row, with new rows forming directly below. Patches of each size then moved exhaustively over each image and image sample. (*d*) Example of changed image for each object with five pixels replaced, where coordinates indicate location of left-most changed pixel. Similar results are found under different cloud conditions (electronic supplementary material, figures S6 and S8).

the opposite extreme, picking the lowest measured standard deviation, found for the lowest mean intensity measured, would lead to over-sampling or over-resolving noise fluctuations at higher mean intensities by roughly an order of magnitude. Either limiting choice of constant resolution in acoustic intensity is then extremely inefficient. For the optical case of figure 3, a similar situation occurs when system resolution is set to a constant luminance. Signal blurring occurs when the constant is too large and over-resolving noise occurs when it is too small. Both are inefficient, as is any constant resolution setting for all mean luminance values. The smaller scintillation factors obtained for light luminance enable subtler environmental patterns to be discerned.

Practical advantages of the current findings can also be illustrated by quantifying the ability to detect changes in natural sounds and in natural objects illuminated by daylight. The approach

is to apply Neyman–Pearson hypothesis testing assuming the Gaussian model of equation (7.1) for each of the various transformations of sound intensity or light luminance including no transformation. The model assumes perception with constant resolution across the perceived data via constant variance and no correlation across pixels. As demonstrated in previous sections, this model is accurate for variance-stabilizing, log and Fechnerian transformations. For untransformed sound intensity and light luminance, in contrast, the equation (7.1) model inaccurately assumes perception with fixed sensing resolution, and the fit to a Gaussian probability density is not as good. So it is useful to explore the consequences with actual sound intensity and daylight luminance image data.

To investigate change detection, two competing hypotheses are compared. In Hypothesis 1, a change is made to the image of Hypothesis 0 by introduction of different data at certain pixels. The test data $\mathbf{G}_j$ is consistent with Hypothesis 1. For the acoustic examples, the changed data is ambient noise measured just after the given acoustic event sample, with the same temporal sampling and frequency filtering as the unchanged event data. This noise has an intensity that corresponds roughly to the lowest signal intensity measured. For the objects imaged with daylight, the changed data is dark mud of low luminance imaged at the same time as the five objects investigated but spatially distinct from them. The changed pixel section in the acoustic images grows linearly in time from either the beginning or end of the time series as indicated in figure 7*d*. In the luminance images, the changed pixel patch grows linearly in the horizontal until it reaches a length of 10 pixels, then begins another changed row below that of up 10 pixels, and so on forming a patch with up to 30 changed pixels in total. The luminance detections include averaging over results where the changed section is exhaustively moved across the given image. The N_{test} image samples of $\mathbf{G}_j$ used to test the hypotheses are collected independently of the N_{train} samples used to construct the expected images $\bar{\mathbf{G}}_1$ and $\bar{\mathbf{G}}_0$ for Hypotheses 1 and 0, respectively. To be consistent with practical implementations, small sample sizes of N_{train} are used. For the sound intensity examples, $N_{\text{test}} = N - N_{\text{train}}$, where $N_{\text{train}} = 10$ and N is the total number of image recordings for the given acoustic signature (figure 1 and electronic supplementary material, figure S1). Hypothesis testing is carried out repeatedly for all combinations of the N samples of each image leading to samples N_{train} independent of N_{test}. For the luminance examples, hypothesis testing is conducted with $N_{\text{test}} = 4500$ samples, which is half the total number of image measurements, with expected image hypotheses constructed from $N_{\text{train}} = 5$ independent samples taken from the remaining half of the total number of image measurements. This is repeated exhaustively for all non-overlapping consecutive sets of N_{train} samples from the remaining half of image measurements. The results of all such independent tests for a given acoustic signature or luminance object are averaged.

The average true positive detection rate over all false-positive rates from the relation (7.6) decision rule is shown in figure 7*b* for variance-stabilizing-transformed acoustic intensity and in figure 8*b* for variance-stabilizing transformed light luminance. Five examples are shown for each. The average rate is 50% when no pixels are changed. This is expected because the competing hypotheses are the same in this case. As the number of changed pixels grows, the rate follows an increasing trend until saturating at 100%. The trend has some fluctuation and is far more gradual in the acoustic case as seen in figures 7*b* and 8*b*.

The likelihood decision rule of equation (7.6) is similarly applied for all other transformations of sound intensity and light luminance, as well as untransformed intensity and luminance. Results are exhibited in figures 7*c* and 8*c* in terms of the deficit from the average true positive detection rate of the variance-stabilizing-transformed case shown in figures 7*b* and 8*b*. Log, variance-stabilizing and Fechnerian transformations have nearly identical performance. As noted previously, their performance is approximately optimal since they fit the likelihood model of equation (7.1) well for which the decision rule of relation (7.6) is optimal. Detection using this same likelihood model and decision rule with untransformed acoustic intensity and light luminance, in contrast, leads to large deficits in performance relative to that found with log, variance-stabilizing and Fechnerian transformed intensities and luminances. This exemplifies

how the use of constant sensing system resolution across all mean intensities or luminances not only theoretically violates Weber's Law in intensity and luminance resolution, but leads to poor pattern recognition in practice. Detection performance with magnitude estimation transformation is consistently less optimal than log, variance-stabilizing and Fechnerian transformation, but more optimal than with untransformed sound intensity and light luminance. Similar results for luminance images with natural light obtained under different cloud conditions appear in the electronic supplementary material. Examples of $\bar{\mathbf{G}}_1$ for sound intensity data appear in figure 7*d* and in figure 8*d* for the daylight luminance data. Application of the instantaneous image level shift of equation (5.1) has a negligible effect on these hypothesis testing results.

These hypothesis tests quantify the relative advantages of the various sound intensity and light luminance transformations investigated, including no transformation. The tests compare how reliably increasingly subtle pattern changes can be detected in each case. The changed visual patch, for example, could contain information about a potential food source or harmful pest. The sudden acoustic signature truncation to background noise, for example, could contain information about an animal tactically freezing after being suddenly alerted to the presence of danger or prey. Both the visual patch change and acoustic signature truncation would be lost in natural signal-dependent fluctuations, go frequently undetected and so lead to potentially significant disadvantages to organisms, systems or machines that do not employ variance-stabilizing, log, Fechnerian transformation of intensity and luminance before pattern matching, or the equivalent. Again, the optimally performing transformations and corresponding estimators and detection decision rules are consistent with sensing system resolution that obeys Weber's Law in perception of sound intensity and light luminance.

From another perspective, the consequences of not transforming intensity in the manner found to be optimal here in pattern matching, or not employing some equivalent sensing system adaptation or tuning to the underlying scintillation statistics of natural terrestrial light and sound, are severe. Optimal pattern recognition would require expensive sampling and learning of the higher statistical moments of every signal pattern to be recognized due to the inherent signal-dependent noise of the intensity scintillation at each pixel in an image. This extensive sampling and training requirement is impractical in a hostile or highly competitive environment where rapid and accurate sensing is essential. It is also unnecessary given the advantageous properties of the simple intensity transformations described here.

9. Conclusion

For organisms, systems and machines that rely on visual and auditory sensory perception to survive or function effectively in their environment, efficient resolution of natural light and sound intensity is essential. This resolution obeys Weber's Law when the smallest resolvable change in the intensity stimulus, a just-noticeable-difference, is not constant but grows in direct proportion to the stimulus. Here, Weber's Law is found to be a consequence of attaining the theoretical minimum mean-square error possible, the Cramer–Rao lower bound, in resolving the intensity of naturally scintillating light and sound. The finding is based on statistics from thousands of measurements of naturally scintillating environmental light and sound signals. Remarkably, just-noticeable-differences in light and sound intensity measured over decades of psychophysical experiments with artificial sources are also found to approximately attain these same respective Cramer–Rao lower bounds. As change-detection thresholds, the just-noticeable-differences are found to be in the optimal range of primarily rejecting natural fluctuations rather than true changes in the mean intensity of our environmental light and sound data. Human intensity resolution is in this way found to be optimally adapted to the natural scintillation of light and sound.

The reliable recognition of patterns imbedded in the scintillating intensities of natural light and sound is also indispensable for survival or proper function in many contexts. Pattern recognition by simple matched-filter correlation between measured and hypothetical images cancels natural scintillation. For intensity perception obeying Weber's Law, this is found to

be advantageous and statistically optimal because perceived scintillation is independent of the underlying signal pattern. For perception with constant intensity resolution, however, it is highly suboptimal because perceived scintillation contains signal information that is then destroyed. This is demonstrated with a variety of examples using natural objects imaged in daylight and sounds made from natural sources. Important environmental patterns are found to be lost in natural scintillation when intensity perception does not follow Weber's Law. Perception with log-transformed intensity is particularly advantageous for a number of reasons. It entails Weber's Law in intensity resolution with the benefit of also having statistically optimal resolution that is constant in the perceived variable. In sensing with natural light and sound, these findings provide a statistical foundation for Fechner's conjecture that just-noticeable-differences in the variable perceived by a human subject should be constant. Log-transformed intensity also tends to converge to a normal probability density as a consequence of the central limit theorem given the natural physical processes causing intensity scintillation. This convergence facilitates advantageous adaptation to natural environmental intensity scintillation by a simple transformation. For example, statistically optimal pattern recognition is achieved by using log-transformed intensity as the perceived variable in matched-filter correlation. For biological organisms, this advantageous adaptation could evolve with natural selection to provide improved intensity resolution and improved pattern recognition in sensing with natural light and sound. Along these lines, it has become standard practice to analyse scintillating light and sound intensity data after log-transformation by use of decibel units, in many scientific and engineering disciplines. This has the advantages and optimal statistical properties presented here.

Data accessibility. All data are available in the main text or the electronic supplementary material [75].

Authors' contributions. S.P.: data curation, formal analysis, investigation, methodology, software, validation, visualization, writing—review and editing; A.K.: data curation, formal analysis, investigation, methodology, software, validation, visualization, writing—review and editing; B.C.: data curation, formal analysis, investigation, methodology, software, validation, visualization, writing—review and editing; N.C.M.: conceptualization, data curation, formal analysis, funding acquisition, investigation, methodology, project administration, resources, software, supervision, validation, visualization, writing—original draft, writing—review and editing.

All authors gave final approval for publication and are responsible for the work performed therein.

Conflict of interest declaration. We declare we have no competing interests.

Funding. This work was funded by MIT Bose Fellowship, William I. Koch Professor of Marine Technology Chair and Massachusetts Institute of Technology.

References

1. Fechner GT. 1860 *Elemente der Psychophysik*, vol. 2. Wiesbaden, Germany: Breitkopf u. Härtel.
2. Miller GA. 1947 Sensitivity to changes in the intensity of white noise and its relation to masking and loudness. *J. Acoust. Soc. Am.* **19**, 609–619. (doi:10.1121/1.1916528)
3. Viemeister NF. 1974 Intensity discrimination of noise in the presence of band-reject noise. *J. Acoust. Soc. Am.* **56**, 1594–1600. (doi:10.1121/1.1903483)
4. Moore BCJ, Raab DH. 1975 Intensity discrimination for noise bursts in the presence of a continuous, bandstop background: effects of level, width of the Bandstop, and duration. *J. Acoust. Soc. Am.* **57**, 400–405. (doi:10.1121/1.380455)
5. Raab DH, Goldberg IA. 1975 Audotory intensity discrimination with bursts of reproducible noise. *J. Acoust. Soc. Am.* **57**, 437–447. (doi:10.1121/1.380467)
6. Houtsma AJM, Durlach NI, Braida LD. 1980 Intensity perception XI. Experimental results on the relation of intensity resolution to loudness matching. *J. Acoust. Soc. Am.* **68**, 807–813. (doi:10.1121/1.384819)
7. Koenig A, Brodhun E. 1888 Experimentelle Untersuchungen über die psychophysische Fundamentalformel in Bezug auf den Gesichtssinn. *Sitzungssberichte preussischen Akademie der Wissenschaften* **37**, 917–931.
8. Hecht S. 1934 A theoretical basis for intensity discrimination in vision. *Proc. Natl Acad. Sci. USA* **20**, 644–655. (doi:10.1073/pnas.20.12.644)

9. Craik KJW. 1938 The effect of adaptation on differential brightness discrimination. *J. Physiol.* **92**, 406–421. (doi:10.1113/jphysiol.1938.sp003612)
10. Blackwell HR. 1946 Contrast thresholds of the human eye. *J. Opt. Soc. Am.* **36**, 624–643. (doi:10.1364/JOSA.36.000624)
11. Cornsweet TN, Pinsker HM. 1965 Luminance discrimination of brief flashes under various conditions of adaptation. *J. Physiol.* **176**, 294–310. (doi:10.1113/jphysiol.1965.sp007551)
12. Davson H. 1980 *Physiology of the eye*, 4th edn. New York, NY: Academic Press.
13. Moore BCJ. 2012 *An introduction to the psychology of hearing*. Leiden, Netherlands: Brill.
14. Lamb TD. 2011 Light adaptation in photoreceptors. In *Adler's physiology of the eye: expert consult* (eds LA Levin, SF E Nilsson, J Ver Hoeve, S Wu, PL Kaufman, A Alm), 11th edn, pp. 429–442. Philadelphia, PA: Saunders/Elsevier.
15. Green DM, Swets JA. 1966 *Signal detection theory and psychophysics*, vol. 1. New York, NY: Wiley.
16. Akre KL, Johnsen S. 2014 *Psychophysics and the evolution of behavior*. Amsterdam, Netherlands: Elsevier Ltd.
17. LaBarbera K, Nelson PB, Bee MA. 2020 Mate choice and the 'opposite miss' to Weber's law: proportional processing governs signal preferences in a treefrog. *Anim. Behav.* **168**, 199–209. (doi:10.1016/j.anbehav.2020.08.014)
18. Strohbehn JW. 1978 Modern theories in the propagation of optical waves in a turbulent medium. In *Laser beam propagation in the atmosphere* (ed. JW Strohbehn), pp. 45–106. Berlin, Heidelberg: Springer.
19. van de Hulst HC. 1981 *Light scattering by small particles*. North Chelmsford, MA: Courier Corporation.
20. Dravins D, Lindegren L, Mezey E, Young AT. 1997 Atmospheric intensity scintillation of stars. I. Statistical distributions and temporal properties. *Publ. Astron. Soc. Pacific* **109**, 173–207. (doi:10.1086/133872)
21. Wessely HW, Mitchell MP. 1971 Solar-scintillation measurements. *J. Opt. Soc. Am.* **61**, 242–247. (doi:10.1364/JOSA.61.000242)
22. Rayleigh L. 1880 XII. On the resultant of a large number of vibrations of the same pitch and of arbitrary phase. *Lond. Edinb. Dublin Phil. Mag. J. Sci.* **10**, 73–78. (doi:10.1080/14786448008626893)
23. Dodge Y, Commenges D. 2006 *The Oxford dictionary of statistical terms*. Oxford, UK: Oxford University Press on Demand.
24. Bartlett MS. 1947 The use of transformations. *Biometrics* **3**, 39–52. (doi:10.2307/3001536)
25. Curtiss JH. 1943 On transformations used in the analysis of variance. *Ann. Math. Stat.* **14**, 107–122. (doi:10.1214/aoms/1177731452)
26. Mitchell RL. 1968 Permanence of the log-normal distribution. *J. Opt. Soc. Am.* **58**, 1267–1272. (doi:10.1364/JOSA.58.001267)
27. Krantz DH. 1971 Integration of just-noticeable differences. *J. Math. Psychol.* **8**, 591–599. (doi:10.1016/0022-2496(71)90008-3)
28. Riesz RR. 1933 The relationship between loudness and the minimum perceptible increment of intensity. *J. Acoust. Soc. Am.* **4**, 211–216. (doi:10.1121/1.1915601)
29. Murray DJ. 1993 A perspective for viewing the history of psychophysics. *Behav. Brain Sci.* **16**, 115–137. (doi:10.1017/S0140525X00029277)
30. Rao CR. 1973 *Linear statistical inference and its applications*. New York, NY: Wiley.
31. Rao CR. 1945 Information and the accuracy attainable in the estimation of statistical parameters. *Bull. Calcutta Math. Soc.* **37**, 81–91.
32. Cramer H. 1946 *Mathematical methods of statistics*. Princeton, NJ: Princeton University Press.
33. Fisher RA. 1925 Theory of statistical estimation. *Math. Proc. Cambridge Philos. Soc.* **22**, 700–725. (doi:10.1017/S0305004100009580)
34. Fisher RA. 1934 Probability likelihood and quantity of information in the logic of uncertain inference. *Proc. R. Soc. Lond. A* **146**, 1–8.
35. Fisher RA. 1934 *Statistical methods for research workers*, 5th edn. Edinburgh and London, UK: Oliver and Boyd.
36. Di Franco JV, Rubin WL. 1968 *Radar detection*. Englewood Cliffs, NJ: Prentice-Hall.
37. Neyman J, Pearson ES. 1933 IX. On the problem of the most efficient tests of statistical hypotheses. *Phil. Trans. R. Soc. Lond. A* **231**, 289–337.
38. Geisler WS, Diehl RL. 2003 A Bayesian approach to the evolution of perceptual and cognitive systems. *Cogn. Sci.* **27**, 379–402. (doi:10.1207/s15516709cog2703_3)

39. Simoncelli EP, Olshausen BA. 2001 Natural image statistics and neural representation. *Annu. Rev. Neurosci.* **24**, 1193–1216. (doi:10.1146/annurev.neuro.24.1.1193)
40. Purves D, Lotto RB. 2011 *Why we see what we do redux: a wholly empirical theory of vision*. Sunderland, MA: Sinauer Associates.
41. Nundy S, Purves D. 2002 A probabilistic explanation of brightness scaling. *Proc. Natl Acad. Sci. USA* **99**, 14 482–14 487. (doi:10.1073/pnas.172520399)
42. Ruderman D, Bialek W. 1993 Statistics of natural images: scaling in the woods. In *Advances in neural information processing systems* (eds J Cowan, G Tesauro, J Alspector), vol. 6, pp. 551–558. San Mateo, CA: Morgan-Kaufmann.
43. Attias H, Schreiner C. 1996 Temporal low-order statistics of natural sounds. In *Advances in neural information processing systems* (eds MC Mozer, M Jordan, T Petsche), vol. 9, pp. 27–33. Cambridge, MA: MIT Press.
44. Mante V, Frazor RA, Bonin V, Geisler WS, Carandini M. 2005 Independence of luminance and contrast in natural scenes and in the early visual system. *Nat. Neurosci.* **8**, 1690–1697. (doi:10.1038/nn1556)
45. Sebastian S, Abrams J, Geisler WS. 2017 Constrained sampling experiments reveal principles of detection in natural scenes. *Proc. Natl Acad. Sci. USA* **114**, E5731–E5740. (doi:10.1073/pnas.1619487114)
46. Laughlin S. 1981 A simple coding procedure enhances a neuron's information capacity. *Z Naturforsch C Biosci.* **36**, 910–912. (doi:10.1515/znc-1981-9-1040)
47. Baddeley R, Abbott LF, Booth MC, Sengpiel F, Freeman T, Wakeman EA, Rolls ET. 1997 Responses of neurons in primary and inferior temporal visual cortices to natural scenes. *Proc. Biol. Sci.* **264**, 1775–1783. (doi:10.1098/rspb.1997.0246)
48. Attias H, Schreiner C. 1997 Coding of naturalistic stimuli by auditory midbrain neurons. In *Advances in neural information processing systems*, (eds M Jordan, M Kearns, S Solla), vol. 10, pp. 103–109. Cambridge, MA: MIT Press.
49. Fastl H, Zwicker E. 2006 *Psychoacoustics: facts and models*, vol. 22. Berlin, Germany: Springer Science & Business Media.
50. Marks LE. 1980 Binaural summation of loudness: noise and two-tone complexes. *Percept. Psychophys.* **27**, 489–498. (doi:10.3758/BF03198676)
51. Scharf B, Fishken D. 1970 Binaural summation of loudness: reconsidered. *J. Exp. Psychol.* **86**, 374–379. (doi:10.1037/h0030159)
52. Stevens SS, Guirao M. 1962 Loudness, reciprocality, and partition scales. *J. Acoust. Soc. Am.* **34**, 1466–1471. (doi:10.1121/1.1918370)
53. Moore BCJ, Glasberg BR. 1983 Suggested formulae for calculating auditory-filter bandwidths and excitation patterns. *J. Acoust. Soc. Am.* **74**, 750–753. (doi:10.1121/1.389861)
54. Gelfand SA. 2017 *Hearing: an introduction to psychological and physiological acoustics*. Boca Raton, FL: CRC Press.
55. Krueger LE. 1989 Reconciling fechner and stevens: toward a unified psychophysical law. *Behav. Brain Sci.* **12**, 251–267. (doi:10.1017/S0140525X0004855X)
56. ISO 226:2003 2003 *Acoustics: Normal Equal-loudness-level Contours*. Geneva, Switzerland: International Organization for Standardization.
57. Stevens JC, Stevens SS. 1963 Brightness function: effects of adaptation. *J. Opt. Soc. Am.* **53**, 375–385. (doi:10.1364/JOSA.53.000375)
58. Stevens SS. 1955 The measurement of loudness. *J. Acoust. Soc. Am.* **27**, 815–829. (doi:10.1121/1.1908048)
59. Onley JW. 1960 Light adaptation and the brightness of brief foveal stimuli. *J. Opt. Soc. Am.* **51**, 667–673. (doi:10.1364/JOSA.51.000667)
60. Hood DC, Finkelstein MA. 1986 Sensitivity to light. In *Handbook of perception and human performance* (eds K Boff, L Kaufman, J Thomas), vol. 1, Sensory processes and perception. New York, NY: Wiley.
61. Levin LA, E Nilsson SF, Ver Hoeve J, Wu S, Kaufman PL, Alm A. 2011 Adler's Physiology of the Eye: Expert Consult, 11Th edn. Philadelphia PA: Saunders/Elsevier.
62. Gloriani AH, Matesanz BM, Barrionuevo PA, Arranz I, Issolio L, Mar S, Aparicio JA. 2016 Influence of background size, luminance and eccentricity on different adaptation mechanisms. *Vis. Res.* **125**, 12–22. (doi:10.1016/j.visres.2016.04.008)
63. Kolmogorov A. 1933 Sulla determinazione empirica di una lgge di distribuzione. *Inst Ital Attuari Giorn* **4**, 83–91.

64. Smirnov N. 1948 Table for estimating the goodness of fit of empirical distributions. *Ann. Math. Stat.* **19**, 279–281. (doi:10.1214/aoms/1177730256)
65. Makris NC. 1996 The effect of saturated transmission scintillation on ocean acoustic intensity measurements. *J. Acoust. Soc. Am.* **100**, 769–783. (doi:10.1121/1.416239)
66. Makris NC. 1995 A foundation for logarithmic measures of fluctuating intensity in pattern recognition. *Opt. Lett.* **20**, 2012–2014. (doi:10.1364/OL.20.002012)
67. Seykora EJ. 1993 Solar scintillation and the monitoring of solar seeing. *Sol. Phys.* **145**, 389–397. (doi:10.1007/BF00690664)
68. Georgobiani D, Kuhn JR, Beckers JM. 1995 Using eclipse observations to test scintillation models. *Sol. Phys.* **156**, 1–5. (doi:10.1007/BF00669570)
69. Shapley R, Enroth-Cugell C. 1984 Chapter 9 Visual adaptation and retinal gain controls. *Prog. Retin. Eye Res.* **3**, 263–346. (doi:10.1016/0278-4327(84)90011-7)
70. Box GEP, Jenkins GM, Reinsel GC, Ljung GM. 2015 *Time series analysis: forecasting and control*. Hoboken, NJ: John Wiley & Sons.
71. Rieke F, Rudd ME. 2009 The challenges natural images pose for visual adaptation. *Neuron* **64**, 605–616. (doi:10.1016/j.neuron.2009.11.028)
72. Graham CH, Brown RH, Mote FA. 1939 The relation of size of stimulus and intensity in the human eye: I. Intensity thresholds for white light. *J. Exp. Psychol.* **24**, 555. (doi:10.1037/h0060530)
73. Lauwereyns J. 2012 *Brain and the gaze: on the active boundaries of vision*. Cambridge, MA: MIT Press.
74. Kay SM. 1993 *Fundamentals of statistical signal processing: estimation theory*. Hoboken, NJ: Prentice-Hall Inc.
75. Pednekar S, Krishnadas A, Cho B, Makris NC. 2023 Weber's Law of perception is a consequence of resolving the intensity of natural scintillating light and sound with the least possible error. Figshare. (doi:10.6084/m9.figshare.c.6472407)